designs

MDPI

Article

Design of a Low-Cost and Low-Power LoRa-Based IoT System for Rockfall and Landslide Monitoring

Luis Miguel Pires [1,2,*] and Ileida Veiga [1,*]

[1] Department of Electronical Engineering, Telecommunications and Computers (DEETC), Instituto Superior de Engenharia de Lisboa (ISEL), 1959-007 Lisbon, Portugal
[2] Technologies and Engineering School (EET), Instituto Politécnico da Lusofonia (IPLuso), 1700-098 Lisbon, Portugal
* Correspondence: luis.pires@ipluso.pt (L.M.P.); a50069@alunos.isel.pt (I.V.)

Abstract

This work presents the development and evaluation of a low-cost and low-power IoT system for monitoring slope instabilities, rockfalls, and landslides using LoRa communication. The prototype integrates commercial ESP32-based hardware with an SX1276 transceiver, a triaxial MEMS accelerometer, and a GPS module for real-time tilt and location measurements. A tilt-estimation expression was derived from accelerometer data, enabling adaptation to different terrain inclinations. Laboratory tests were performed to validate the stability and accuracy of the inclination measurement, followed by outdoor LoRa range tests under mixed line-of-sight conditions. A lightweight dashboard was implemented for real-time visualization of GPS position, signal quality, and tilt data. The results show reliable tilt detection, consistent long-range communication, and low power consumption, highlighting the potential of the proposed prototype as a scalable and energy-efficient tool for geotechnical monitoring.

Keywords: IoT monitoring system; IoT detection node; LoRa/LoRaWAN; landslide detection; remote geological monitoring

Academic Editor: Bhanu Shrestha

Received: 5 November 2025
Revised: 8 December 2025
Accepted: 10 December 2025
Published: 12 December 2025

Citation: Pires, L.M.; Veiga, I. Design of a Low-Cost and Low-Power LoRa-Based IoT System for Rockfall and Landslide Monitoring. *Designs* **2025**, *9*, 144. https://doi.org/10.3390/designs9060144

1. Introduction

Monitoring slope instabilities is essential for mitigating risks to populations and infrastructure, especially in regions where geological and climatological factors increase susceptibility to mass-movement events. Slopes are extensive, and soil types are variable and often cause a state of instability, for example, in Portugal, which makes the country particularly prone to landslides and rockfalls; the combination of these factors is evidenced by the following unfortunate events that have occurred over time:

- Slide on housing, leading to the destruction of houses in the city of Esposende, Portugal, in 2022 [1].
- Landslide at the quarry's brink, leading to the collapse of a municipal road, carrying away vehicles and resulting in five deaths in the city of Borba, Portugal, in 2018 [1].
- Landslide on the A9 highway. No fatalities or injuries, but traffic disruption for weeks in the Lisbon Metropolitan Area in 2010 [1].
- Numerous landslides caused damage to homes and roads, and four fatalities in the Lisbon Metropolitan Area, the city of Régua, and the city of Santa Marta de Penaguião in 2001, among many other incidents that have taken place and continue to happen nowadays [1].

- Landslides in Serra da Estrela, Portugal, in 2022 that cleared the way for trees, cars, and lampposts and damaged a vast range of infrastructures [2].

The mentioned incidents pointed out the necessity of monitoring mechanisms that are both efficient and very early in detecting that slope movements have happened. The evacuation of first-generation bridges is a preferred option, certainly in addition to other potentially conceited points and good ethical rates. Apart from these happenings, a few geological and climatological factors are the reason why Portugal is so prone to landslides. Most of the steep slopes in the North and the Center of the country rest on a granite massif that is badly cracked or on a schist that has low cohesion, which, after the heavy rains, easily loses stability. Furthermore, winter months bring beautiful, but very heavy rains that are often above the European average, which leads to rapid soil saturation and increases the probability of both surface and deep rupture. Under such conditions, these places become very attractive for the assessment of LoRa-based early warning systems because they are characterized by rough and inaccessible terrain as well as by the necessity for real-time remote monitoring.

On this note, LoRa technology has been seen as a viable option for tracking rockfall and landslide events. LoRa technology, together with the Long-Range Wide-Area Network (LoRaWAN) protocol, makes it possible to set up wireless sensor networks that can operate in very remote and inaccessible areas. The technology's major benefits are over-the-air communication (3–4 km range in urban settings and over 12 km range or more in sparsely populated places), very little energy consumption, and lower spending on both installation and maintenance [3].

This article begins by presenting the state of the art and related works in Section 2. Section 3, materials and methods for our experience, and Section 4, achieved results, are presented. Section 5 presents the conclusion of the study along with considerations and directions for future work.

2. State of the Art and Related Works

This section presents the current state of the art, in Section 2.1, and in Section 2.2, some related works about the topic of study.

2.1. State of the Art

In the present study, the reference made was to a sensor network composed of IoTs that could collect and send environmental data nonstop. The whole process makes the environment that comprises isolated devices to be that of intelligent, networked systems that can communicate with each other either automatically or share time in larger digital ecosystems [4].

IoT has changed the way people, infrastructures, and nature coexist by allowing universal data collection and connectivity. The aforementioned technologies make it possible to create such systems that are flexible in their operation, consume very little energy, and are able to quickly adapt to environmental fluctuations [5].

Up until now, company adoption of IoT technologies has steadily grown for industrial, urban, and environmental applications. According to the present estimates, more than 25 billion active interlinked devices are across the planet, while the figure might go up to over 30 billion by 2030. The usage of these devices is spreading more and more over various sectors like industrial automation, precision agriculture, healthcare, city management, and environmental monitoring [6]. Such dramatic growth has led to the generation of an enormous amount of various types of data, which need sophisticated techniques for handling and analyzing that, in turn, is leading to the amalgamation of IoT with Big Data

Analytics. Tools for analyzing data not only allow measurements to be taken in volume from IoT, but also allow for the detection of relevant models.

The combination of these domains offers such advantages as real-time insights, predictive maintenance, and data-driven optimization—the main facilitators of resilient and adaptive infrastructures.

Geotechnical monitoring systems gain significantly from the integration of IoT sensors and analytics platforms [7,8]. The most common application domains include Smart Cities, Digital Health, Industrial IoT, and Smart Earth systems. In the case of urban areas, IoT networks help improve the management of mobility, the efficiency of energy use, and the safety of the public; in healthcare, wearable and biomedical sensors are used for remote patient monitoring; in industrial settings, Industrial IoT is responsible for more efficient processes and less downtime thanks to real-time data collection; and in the environmental sector, Smart Earth frameworks are composed of thousands of distributed sensors in land, water, and air to detect and respond to ecological risks and natural disasters.

In the recent past, one of the things that helped wireless sensor networks was their use for the early detection and mitigation of environmental hazards. Some of those environmental hazards are wildfires, landslides, and rockfalls. Wireless sensor networks possess the major advantages of scalability, energy efficiency, and cost-effectiveness, especially in the case of their being deployed in remote or hard-to-access locations as compared to the traditional systems: human observation, satellite imaging, or camera surveillance [9].

A significant recent contribution to this field is the study in [10], which demonstrates the feasibility of integrating LoRa-based wireless networks for real-time geotechnical hazard monitoring. The authors developed a distributed network of sensor nodes equipped with accelerometers and LoRa transceivers capable of detecting soil movements and rock instabilities, transmitting alerts over long distances with minimal power consumption. Their work exemplifies how LoRa technology, when coupled with efficient sensor architectures, enables reliable and long-range communication in challenging terrains.

Hence, the joint evolution of these technologies has yielded more reliable and energy-efficient systems for environmental monitoring. The IoT, LoRa, and wireless sensor networks merge together, creating a strong platform that supports the development of systems that are continuous in operation and efficient in power utilization for data acquisition. These types of systems are of great use not only to the prevention of disasters through early-warning systems but also to the sustainable management of the environment and infrastructure by means of predictive analysis and adaptive strategies.

2.2. Related Works

A thorough evaluation of all monitoring systems based on wireless sensor networks for landslides and rockfalls is presented in this article [9], which investigates the hardware design as well as the IoT communication infrastructure. The authors organize over 100 journal articles and pinpoint the major technological advances in the domain. One of the major points of the study is the increased use of low-power microcontrollers (MCUs) (e.g., ESP32, STM32L4, and ATmega328P) together with LoRa SX1276/78 radios, which have proved to be very durable in both star and mesh topologies. Triaxial accelerometers (ADXL345, MPU6050), Micro-Electro-Mechanical Systems inclinometers, SCA103T, and soil moisture and pressure sensors (BME280 and YL-69) are some of the most frequently mentioned sensors. The paper that explores the hybrid communication architectures, namely, LoRa–Wi-Fi and LoRaWAN, and puts a strong emphasis on the adoption of Raspberry Pi-based gateways and the use of cloud platforms such as ThingSpeak, The Things Network (TTN), and Amazon Web Services (AWS) IoT Core for integration. Speaking of performance, the study shows that LoRa technology allows operation at distances ranging from 2 to

8 km while still drawing less than 50 mA during transmission; hence, several months of operation are possible with a 3.7 V/2000 mAh Li-Ion battery. Moreover, the authors claim that natural evolution will be the incorporation of embedded TinyML for real-time anomaly detection, which will minimize the need for continuous data transmission and will, thus, improve the energy efficiency of the field nodes.

The paper introduced in [10] describes a geotechnical monitoring system that employs LoRaWAN and was set up in the field of a whole hill. The sensor's nodes were constructed using an STM32L071 microcontroller and SX1272 radio module set to SF10/BW125 kHz. Along with the STM32L071 and SX1272, packaged IP67 housings, which allow for outdoor use, were sensors like the LIS3DH Micro-Electro-Mechanical Systems accelerometer, NXP MMA8451 tilt sensor, and Bosch BMP180 temperature/pressure sensor, etc. A solar panel of 5 W together with a 2200 mAh Li-Po battery is used for power, and charge is managed via the Maximum Power Point Tracker (MPPT) BQ24074 technology, which can give autonomy of up to 6 months. The network is arranged in a star formation, with a gateway that is based on Raspberry Pi 4, which has an iC880A HAT concentrator attached to it and is running ChirpStack as the network server. Data is collected at the local site and sent through 4G to a Node-RED Dashboard web application. Packet delivery ratio > 95% was confirmed during the test at 3 km line of sight with SNR > 7 dB. The article proves that the combination of super low-power microcontrollers with portable LoRaWAN provides outstanding energy efficiency and strong coverage for temporary or permanent monitoring in difficult areas.

In their article [11], Muladi et al. detail the creation of a cost-effective early warning system designed for landslide-prone areas. Their work addresses a critical gap by offering a solution that is both affordable and suitable for remote locations with limited infrastructure, overcoming the cost and complexity barriers of existing systems. The system architecture integrates a soil moisture sensor, an MPU6050 accelerometer for tilt detection, and a NEO 6M GPS for location, with a TTGO LoRa32 module. Data from these sensors is wirelessly transmitted to a gateway using the long-range, low-power LoRaWAN protocol and is subsequently relayed to the Blynk application for real-time monitoring and alerting. A significant aspect of their research was the performance analysis of the LoRaWAN network. By testing different Spreading Factors (SFs) across various distances, they determined that SF12 provides the most reliable communication for ranges up to 300 m, as it ensures a high packet delivery ratio, even though it results in a slightly longer Time on Air (ToA). Operationally, the system functions in two distinct modes: a Scheduling Mode for periodic data updates and an Emergency Mode that activates instantly when predefined thresholds for slope (>20°) and soil moisture (>60%) are breached. Through comprehensive testing, the authors successfully validated the system's accuracy, its end-to-end data pipeline, and its ability to generate timely alerts, establishing it as a practical and robust tool for landslide risk mitigation.

In their article [12], Muladi et al. present an advanced landslide monitoring system that utilizes the ChirpStack platform to manage a LoRaWAN network, enhancing rapid response and energy efficiency in remote, infrastructure-scarce regions of Indonesia.

The system architecture employs a star topology with two types of sensor nodes: weather nodes (measuring rainfall, wind speed, temperature, etc.) and ground nodes (equipped with soil moisture, accelerometer, gyroscope, and magnetometer sensors to detect soil movement and position shifts). A key innovation is the use of inertial sensors (accelerometers) to detect ground displacement within 0.17 s, significantly faster than relying solely on GPS. Data from these nodes is transmitted to a ChirpStack-based gateway and then forwarded to a cloud server for real-time monitoring via a Grafana dashboard. The research highlights the performance of LoRa communication, testing different SF and finding that data transmission is faster at night (ToA as low as 0.17 s for SF7) compared to

daytime. The system was successfully deployed in a landslide-prone area in Songgokerto Village, using six ground nodes and three weather nodes. The authors conclude that the integration of the ChirpStack platform provides a reliable, low-power, and cost-effective solution for real-time landslide monitoring, contributing significantly to early warning and disaster mitigation efforts.

In their article [13], Wang et al. propose a landslide monitoring system that utilizes LoRa wireless technology to overcome the limitations of traditional systems, such as high-power consumption, limited transmission distance, and inability to perform real-time monitoring in complex mountainous terrain. The system architecture is based on a star topology and consists of a collection of sub-nodes and a gateway master node. The sub-nodes, built around an STM32 microcontroller, integrate sensors for rainfall, displacement, and tilt, and communicate with the master node via LoRa (using the SX1278 chip). The data collection method presented in this paper employs an adaptive scheme in which the sampling frequency is changed according to sensor variation. This strategy keeps the system in a low-power state ($\approx$1 mA) under normal conditions and triggers high-frequency transmissions (up to 1 s intervals) only when thresholds are exceeded, balancing energy efficiency with timely capture of critical precursor data. The system was deployed in the Jianshanying landslide area in Guizhou, China. Over nine months, field tests showed reliable triggering of encrypted transmissions during rainfall and notable displacement events (e.g., 86.2 mm). The results also confirm that the architecture maintains low power consumption under stable conditions.

Ragnoli et al. unveil in their publication [14] a structural health monitoring system for cities suffering from landslides. The system's principle is to monitor building tilt and earth movement, which would be an aid to preventive maintenance and evacuation adaptation. It is constructed using a LoRaWAN star topology where the sensor nodes combine Micro-Electro-Mechanical Systems accelerometers (LIS3DHs) and environmental sensors (BME680). The nodes are used to detect tilt and monitor the air quality. Operating with minimal power is at the top of the list when it comes to design considerations. The system uses deep sleep modes along with solar energy harvesting to accomplish this, with an average current consumption of 3.1 mA while active and 50 µA during standby. The Things Network facilitates connectivity, and the Node-RED web dashboard serves the purpose of data visualization for real-time monitoring and alarm management. The paper provides comprehensive validation: power consumption assessment, radio coverage simulations with Longley–Rice, and a real test setting in Bucchianico, Italy. Communication was stable in field tests with the Received Signal Strength Indicator (RSSI) varying between -80 and -107 dBm, and at the same time, structural tilt was effectively monitored. The authors point out the system's modularity, energy efficiency, and its actual usage in urban landslide risk management.

The article [15] presents the concept of a LoRa-based real-time landslide monitoring IoT system that is assessed based on network metrics and energy performance, focusing on the measurement aspect. The prototype is made up of sensor nodes that are based on ESP32-WROOM and have LoRa SX1278 (433 MHz) modules, which work in peer-to-peer mode and in LoRaWAN with a RAK7249 gateway. The types of sensors that were used in this experiment were MPU6050 accelerometers, YL-69 soil moisture sensors, DS18B20 temperature sensors, and SW-420 piezoelectric vibration sensors. The power source for the system is provided by 3.7 V/2500 mAh batteries, which are equipped with 6 V/3 W solar panels. The programming for the firmware was performed in the Arduino IDE with deep sleep mode routines and periodic sampling (every 15 min). The metrics that were evaluated included RSSI (-105 to -125 dBm), SNR (-7 to 12 dB), and average consumption of 35 mA per transmission. The data is forwarded via a messaging server used in the study and was

linked to an InfluxDB database for data storage and Grafana for visualization. The results of the experiments revealed that the spreading factor and bandwidth parameters could greatly affect the battery life of the device (up to 210 days). The authors of the article finally stated that the combination of ESP32 and SX1278 ranks among the best choices for low-cost and modular early warning systems.

In ref. [16], Gamperl et al. introduce an inexpensive and modular IoT geosensor network for landslide warning in advance. The design of each node consists of an ESP8266 microcontroller and incorporates LoRa RFM95W (868 MHz) communication. This is supported by a Raspberry Pi functioning as a LoRa Packet Forwarder and TTN server. Within the nodes, various sensors such as MPU9250, BME280, and DS18B20 are integrated to allow for monitoring of multiple parameters. The energy for the system comes from 6 V/2 W solar panels, a TP4056 regulator, and 2200 mAh Li-Ion batteries that are primarily used in deep sleep and turned on for seismic events to save power. A backend that consists of InfluxDB, Node-RED, and Grafana provides data visualization and alerts to Telegram automatically. Trials conducted in the Bavarian Alps indicated a communication range of more than 4 km, a latency of less than 3 s, and a reliability of over 90%. The authors point out the benefits of the architecture in terms of scalability, simplicity in adding new sensors, and its open-hardware/open-data policy, which together transform the solution into a perfect candidate for educational and community monitoring applications.

In the paper [17], the authors introduce a self-sufficient multi-technology LoRa sensor network that is meant to improve the dependability and the detection of landslides through the application of redundancy. A node in the sensor network is developed around the STM32L0 + MCU, which utilizes SX1276 LoRa radios and nRF52832 Bluetooth low energy for local calibration and control through a smartphone app. LIS3DH Micro-Electro-Mechanical Systems accelerometers, piezoelectric (Murata PKLCS1212E) and capacitance (CapSense VH400) soil moisture sensors, a GNSS module (u-blox NEO-6M) for georeferencing, and an accelerometer are some of the sensors integrated in the system. LoRa is working with 868 MHz, Adaptive Data Rate, and 17 dBm transmission power, while gateways are integrating LoRaWAN with 4G and Wi-Fi backhaul for incident redundancy. Moreover, the network is set up to allow remote updates and the use of priority packet routing techniques. The system operates on a hybrid power source consisting of five W solar panels, supercapacitors, and 3.2 V $LiFePO_4$ batteries with energy management by BQ25570 (energy harvesting IC). Test conducted in the field indicates that the system can stay up and running for more than 9 months, and the time needed to respond when seismic events are simulated is less than 2 s. The authors of the article point out that the system is very reliable under failure of communication, and they rely on cross-synchronization between LoRaWAN and Bluetooth Low Energy (BLE) to support this claim. They also advocate for the incorporation of local inference (edge intelligence) in future versions for predictive detection of geotechnical movements.

Table 1 shows a summary of the relevant research discussed.

Table 1. Summary of the relevant research discussed.

Article	Platform/MCU	IoT Network	Used Sensors	Power/ Battery Capacity	Cost per Node
[10]	STM32L071	LoRa SX1272 (868 MHz); Portable LoRaWAN (ChirpStack)	LIS3DH, MMA8451, BMP180	Solar 5 W Li-Po 2200 mAh	Medium
[11]	STM32F103	LoRa SX1276 (868 MHz); LoRaWAN (TTN backend)	MPU6050, DHT22, YL-69	Solar 10 W Li-Ion 3000 mAh	High

Table 1. *Cont.*

Article	Platform/MCU	IoT Network	Used Sensors	Power/ Battery Capacity	Cost per Node
[12]	ESP32-WROOM	LoRa SX1278 (868 MHz); Portable LoRaWAN (ChirpStack)	BME280, ADXL345, SW-420	Solar 3 W Li-Po 2500 mAh	Medium
[13]	STM32L0	LoRa SX1276 (433 MHz)	MPU6050, BMP280, DS18B20	Battery 3.7 V Li-Ion 2400 mAh	Medium
[14]	ATmega328P	LoRa RFM95W and LoRaWAN (868 MHz)	ADXL345, BME280	Solar 5 W Li-Ion 2000 mAh	Medium
[15]	ESP32-WROOM	LoRa SX1278 (868 MHz); P2P e LoRaWAN (RAK7249)	MPU6050, YL-69, DS18B20, SW-420	Solar 3 W Li-Po 2500 mAh	Low
[16]	ESP8266	LoRa (868 MHz); RFM95W; TTN	MPU9250, BME280, DS18B20	Solar 2 W Li-Ion 2200 mAh	Medium
[17]	nRF52832 (BLE)	LoRa SX1276 (868 MHz) + BLE (dual stack); LoRaWAN + 4G	LIS3DH, PKLCS1212E, VH400, GPS NEO-6M	Solar 5 W $LiFePO_4$ 3.2 V (BQ25570)	Very High
This work	Tx: ESP32-LILYGO T-Beam Rx: Arduino Pro mini	Tx: SX1276 (868 MHz) Rx: LoRa RFM95 (868 MHz); P2P Ngrok dashboard	ADXL335 GPS NEO-6M	Battery 3.7 V Li-Ion 2600 mAh	Very Low (academic prototypes with off-the-shelf components, MCUs, sensors, common transceivers)

The investigation of the years 2021 to 2025 confirmed that the use of LoRa/LoRaWAN as an IoT backbone for geotechnical monitoring was gradually taking place and that the selection of low-power MCUs (STM32, ESP32, and ATmega) and triaxial Micro-Electro-Mechanical Systems sensors was justifiable in terms of their accuracy and cost. The use of hybrid systems, which include LoRa, BLE, and 4G, is increasing, along with the adoption of advanced techniques for energy management (energy harvesting) and the integration of cloud dashboards (TTN, AWS IoT, Node-RED). The duration of battery life commonly ranges between 6 and 12 months, and the distances covered may be more than 3 km as even in rough terrain. Referenced as article [17], this work marks the most advanced stage in the series, where the multi-tech setup, redundancy, and local inference are introduced, which eventually leads to the implementation of predictive detection systems with edge intelligence (Edge AI). Recent studies, as discussed in [18], have again pointed to the ability of lightweight IoT-based monitoring systems by confirming that the use of energy-efficient wireless communication methods can drastically increase the life span of distributed geotechnical sensors. Our method, especially concerning the optimization of sampling, communication parameters, and power consumption, is in agreement with these findings.

3. Materials and Methods

This section is divided into subsections and provides a concise and precise description of the experimental system, hardware integration, and algorithms developed for the transmitter (node) and receiver.

3.1. System Implementation and Hardware Setup

The main emphasis of the article is to develop a node capable of being interlinked with the LoRa network, extending the coverage to extensive coastal areas and mountain slopes, with maybe a few dozen to hundreds of identical nodes for system reliability.

The proposed system architecture is shown in Figure 1. The system consists of two main subsystems: the IoT-Node (Detection node) and the Gateway. The IoT-Node is responsible for collecting data through an accelerometer sensor, which acts as a trigger: whenever movement is detected, the system is activated, and the node sends the geographic coordinates and the location's tilt data to the Gateway via LoRa network. Gateway, in turn, is responsible for receiving the data, displaying it on a HyperText Markup Language (HTML) website, and generating an alert when necessary. The detection node system is composed of the following: LILYGO T-Beam, Shangai, China [19] that uses (embedded) LoRa transceiver SX1276, Semtech, Camarillo, CA, USA [20] operating at 868 MHz and NEO-6M, ublox, Zurich, Switzerland [21]; GPS receiver, also embedded; ADXL335 accelerometer, Analog Devices Inc., Norwood, MA, USA [22]; Battery 18650 [23]. The Gateway system is composed of an Arduino Pro-Mini, Qualcomm, Ivrea, Italy [24], a LoRa module RFM95, Semtech, Camarillo, CA, USA [25], a Battery 18650, a USB interface for a laptop (Intel [26] i3, 8G Random Access Memory (RAM)) with a web interface for a dashboard.

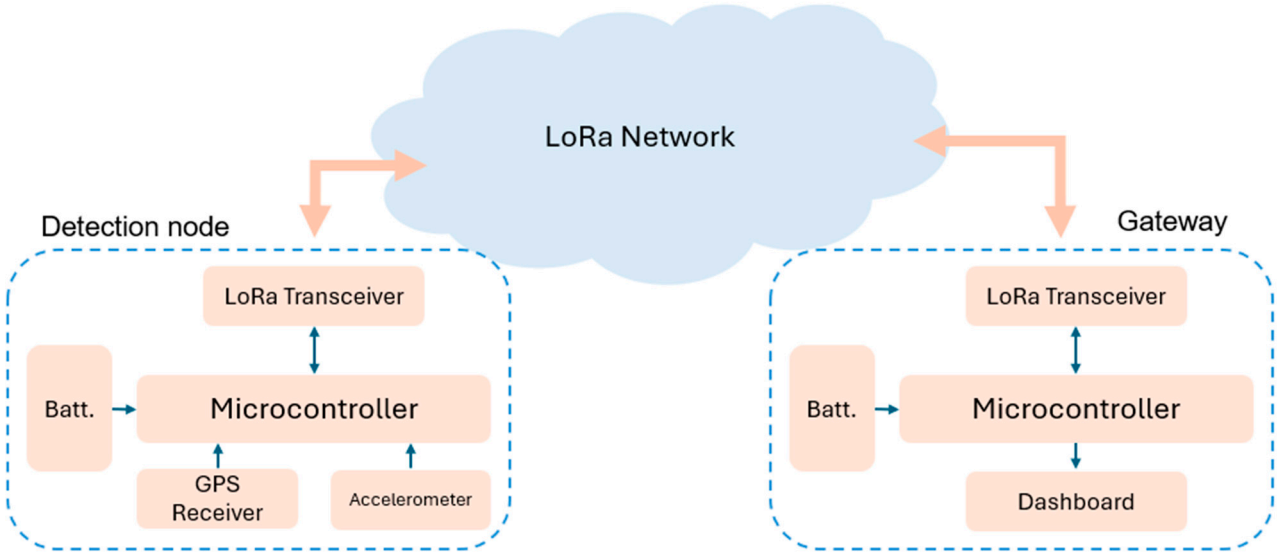

Figure 1. System architecture.

The composition of the IoT detection node is presented in Table 2.

Table 2. IoT-node components.

Component	Description	Model Used
Motion sensor	Used to detect movement or vibrations in the ground	ADXL335
Battery	Power source for autonomous operation	Battery 18650
GPS module	Responsible for recording the exact location of the site	GPS module NEO-6M
Microcontroller	Responsible for processing the acquired data	LillyGO T-Beam
LoRa transceiver	Responsible for sending the acquired data using the LoRa modulation technique	SX1276

The composition of the gateway is presented in Table 3.

Table 3. Gateway components.

Component	Description	Model Used
LoRa Receiver	Responsible for wireless communication with the remote sensor (IoT detection node)	RFM95
Microcontroller	Responsible for receiving data from the IoT detection node and processing it	Arduino Pro Mini
Laptop	It is responsible for converting electrical signals into readable data	Intel i3 8G RAM

The slope thresholds ($\pm 2^{\circ}$) that were adopted are in line with the values mentioned in studies that found the first micro-displacements on unstable slopes, which led to the detection of slight variations without the risk of false positives. The interval of sampling (1 s according to [22]) was estimated as a compromise between the reduction in energy consumption and the adequacy of temporal resolution for the slowest phenomena. The chosen LoRa parameters (SF7-SF12, BW 125 kHz, CR 4/5) correspond to the most widely used configuration in long-range testing and the best tested scenarios, which guarantee that the studies performed before are still comparable. The LoRa parameters in the last tests were as follows: 6 dBm transmission power, SF 8, BW 125 kHz, and CR 4/5.

The transparent character of the methodological decisions made allowed the documentation to be easily available and the experiment to be reproduced without the necessity of the experimental set being increased.

3.1.1. Controllers

The controller used in the experiment for the IoT detection node is the LILYGO T-Beam, which provides an integrated and efficient solution for IoT applications with long-range communication. I chose this platform because it combines the ESP32 Shangai, China [27] microcontroller, the NEO-6M GPS module, Zurich, Switzerland, and the SX1276 LoRa radio, Camarillo, CA, USA, on a single board, simplifying hardware and reducing power consumption. Additionally, its support for an 18650 battery ensures extended autonomy, which is crucial for remote projects. Although the T-Beam does not include an integrated motion sensor, its architecture allows for the easy connection of external sensors, such as accelerometers, via General Purpose Input/Output pins. ESP32 is the "brain" of the LILYGO T-Beam, Shangai, China. It features 448 kB of Read-Only Memory (ROM), 520 kB of Static Random Access Memory (SRAM), and 16 kB of SRAM in the real-time clock. It stands out due to its dual-core 32-bit Xtensa LX6 [28] processor running up to 240 MHz, enabling efficient multitasking, such as simultaneously managing LoRa communications and GPS data processing. This capability makes it ideal for processing location information, managing wireless communication, and integrating potential additional sensors, such as motion sensors connected via General Purpose Input/Output pins. In terms of energy efficiency, the ESP32 offers multiple deep sleep modes (used in firmware of our experience), allowing efficient management of peripherals, such as turning off the GPS when not in use.

The gateway system captures data via LoRa communication using a transceiver. The information is processed by a microcontroller and displayed in real-time on a local web interface implemented in HTML. The controller used in the Gateway is the Arduino Pro Mini. The Arduino Pro Mini is a microcontroller board based on the ATmega328P [29]. It has 14 digital input/output pins (6 of which can be used as Pulse Width Modulation outputs), 6 analog inputs. Arduino Pro Mini can be powered in two ways: via a Future Technology Devices International cable or interface board connected to the 6-pin header, or via a regulated 3.3 V or 5 V power supply (depending on the model, 3.3 V is used in our experiment) connected to the VCC pin. ATmega328P has 32 kB of flash memory for code

storage (with 0.5 kB used by the bootloader). In addition, it features 2 kB of SRAM and 1 kB of Electrically Erasable Programmable Read-Only Memory (EEPROM).

3.1.2. Sensors

The NEO-6M GPS, Zurich, Switzerland belongs to the family of standalone GPS receivers (NEO-6) based on the u-blox 6 positioning engine, combining high performance with affordable cost. Its compact size (16 × 12.2 × 2.4 mm) makes it ideal for mobile devices with space and power constraints [21]. It can be powered by a voltage between 2.7 V and 3.6 V, supports interfaces such as Universal Asynchronous Receiver-Transmitter (UART), Universal Serial Bus (USB), Serial Peripheral Interface (SPI), and Inter-Integrated Circuit (I2C). It includes a real-time clock crystal and 3 configuration pins that are used to set parameters before initialization, as shown in Table 4.

Table 4. GPS pins (adapted from [21]).

Pins	Function	Values
CFG_COM0	Configures the communication interface (protocol and baud rate)	- 1: NMEA (9600 baud) or UBX (57,600 baud) - 0: NMEA (38,400/4800 baud)
CFG_COM1	Complete Communication Setup	- 1 or 0 (combines with CFG_COM0 to define the protocol and baud rate)
CFG_GPS0	Sets the GPS power mode	- 0: Eco Mode (power saving) - 1: Maximum Performance Mode

For the GPS configuration on ESP32, we used pins 34 (RX) and 12 (TX) of the ESP32 to connect to the NEO-6M module, configuring UART with a baud rate of 115,200 using the Hardware Serial library. The configuration was successfully established to receive National Marine Electronics Association (NMEA) data, following the manufacturer's standard.

To extend the capabilities of the IoT detection node, the ADXL335 sensor, Massachusetts, USA, was implemented as an external accelerometer to the LILYGO T-Beam module Shangai, China.

The module was designed to be compatible with protoboards and connects all pins of the ADXL335 to a 6-pin connector with 0.1-inch spacing. These pins include three analog outputs to measure acceleration along the X, Y, and Z axes, two power pins, and a self-test pin. ADXL335 operates with DC voltages from 1.8 V to 3.6 V, with 3.3 V being the typical operating voltage. The module also includes an integrated 3.3 V voltage regulator, which facilitates use with microcontrollers. The sensor is very power efficient, using only about 350 µA during normal operation. ADXL335 can measure acceleration in a range of ±3 G. This means it can detect acceleration up to 3 times the force of gravity in any direction [10]. The ADXL335 output is "ratiometric," meaning the voltage it outputs changes in direct proportion to the acceleration it detects. The sensor was calibrated to exhibit the expected behavior.

The technical specifications are presented in Table 5.

Table 5. Technical specifications (adapted from [22]).

Parameter	Value
Operating voltage [V]	1.8~3.6
Operating current [µA]	350

Table 5. *Cont.*

Parameter	Value
Detection range	±3 g (full scale)
Temperature range	−40 to +85 °C
Sensing axis	3 axes
Sensibility [mV/g]	270 a 330 (ratiometric)
Shock resistance	Up to 10,000 g
Dimension	4 mm × 4 mm × 1.45 mm

In the next paragraphs, we focus on the tilt functionality in accelerometers, finalizing this section with the approach for ADXL335 in the IoT detection node.

Tilt-based sensing relying on low-power triaxial accelerometers is a means of detecting mass movements such as landslides, rockfalls, and soil displacements with high effectiveness. The variations in ground inclination are causing instability, and, accordingly, the continuous monitoring of the angular deviations is providing a basic early warning indicator for geotechnical hazard prevention systems. The proposed system of monitoring is based on the method of gravitational acceleration vector measurement and its projection onto the sensor's orthogonal axes. The tilt that is measured is compared with a reference inclination that has been established beforehand, thus enabling the identification of micro-deformations and slope displacements with high temporal resolution [30–32].

A module like the ADXL335 [22] is a Micro-Electro-Mechanical Systems capacitive accelerometer that can measure the acceleration on all three corners of axes, X, Y, and Z, which are mutually orthogonal to each other. The acceleration in that direction generates an analog voltage on each axis, which is proportional to the respective acceleration component.

The gravitational acceleration $\vec{g}$, let g equal to 9.8 m/s^2, is the only acceleration that acts on the accelerometer when it is under static conditions (i.e., at rest, no motion or vibration). The sensor does not measure the angle of inclination directly, but it does measure the component of the gravity vector along its axes. Thus, the output of the accelerometer corresponds to the following [30–32]:

$$\vec{a} = (a_x, a_y, a_z) \tag{1}$$

The three components show the projection of gravitational acceleration on the respective axis. In the non-moving situation, the accelerometer can measure the gravitational vector, which can be written as [30–32]

$$\vec{g} = (a_x, a_y, a_z) \tag{2}$$

with a constant magnitude of [30–32]

$$\left|\vec{g}\right| = \sqrt{a_x^2 + a_y^2 + a_z^2} = g \tag{3}$$

If the accelerometer is perfectly horizontal, the entire gravity vector acts along the Z-axis [30–32]:

$$a_x = 0, a_y = 0, a_z = g$$

But, if the sensor is tilted at an angle θ_x concerning the X-axis, the gravitational acceleration vector has a component along the X-axis, which causes the Z-axis component to reduce. The components' correlation establishes the tilt angle. Considering vector geometry,

the scalar product gives the cosine of the angle between the gravitational acceleration vector $\vec{g}$ and the unit vector along the X-axis $\hat{i}$ [30–32],

$$\cos(\theta_x) = \frac{\vec{g} \cdot \hat{i}}{|\vec{g}||\hat{i}|} \tag{4}$$

Since $\vec{g} \cdot \hat{i} = a_x$ and $|\hat{i}| = 1$,

$$\cos(\theta_x) = \frac{a_x}{|\vec{g}|} \tag{5}$$

Substituting the magnitude of the gravitational vector $|\vec{g}|$ [30–32],

$$\cos(\theta_x) = \frac{a_x}{\sqrt{a_x^2 + a_y^2 + a_z^2}} \tag{6}$$

Applying the inverse cosine gives the tilt angle in radians [30–32],

$$\theta_x = \cos^{-1}\left(\frac{a_x}{\sqrt{a_x^2 + a_y^2 + a_z^2}}\right) \tag{7}$$

To express this angle in degrees, the conversion factor $\frac{180}{\pi}$ is applied [30–32],

$$INC_x = \frac{180}{\pi} \cdot cos^{-1}\left(\frac{a_x}{\sqrt{a_x^2+a_y^2+a_z^2}}\right) \tag{8}$$

The derivation presented in Equations (1)–(8) follows the standard vector-projection method widely described in the literature for static tilt estimation using triaxial accelerometers [30–32].

The inclination of the sensor with respect to the X-axis is expressed by this equation. The same argument is valid for the Y and Z axes, giving rise to the respective angles, INC_y and INC_z. When the accelerometer lies flat, $a_z \approx g$, while $a_x \approx a_y \approx 0$, resulting in $INC_z \approx 0°$. As the sensor is tilted, the projections a_x, a_y, a_z vary according to the cosine law, and the computed inclination increases proportionally [30–32]. By tracking the evolution of INC_x, INC_y, and INC_z over time, the system can infer multi-axis displacements and detect early deviations that may precede structural or ground failure.

An IoT sensing node's accelerometer, which is typically placed on the retaining or protective barrier, is attached to braided steel cables with mechanical clamps. The microcontroller's Analog-to-Digital Converter (ADC) receives the ADXL335's analog signals, and the local processing computes the tilt angles using Equation (8). Subsequently, the node sends the inclination data via LoRa to a remote monitoring station after being processed.

During the initial topographic and calibration phase, the reference inclination is established, thereby defining the baseline ("zero tilt") for comparison with future measurements. Though theoretical derivation operates under the ideal static conditions, accuracy is affected by several factors during the monitoring [30–32]:

1. Dynamic acceleration interference: Elevation or lowering of the device due to, e.g., vibrations, working on machinery that generates seismic activity, or sudden mechanical shocks are situations that may cause tilt to be falsely read as a temporary shift in the gravity vector. Low-pass filtering (e.g., cutoff frequency below 5 Hz) can be helpful in capturing only the quasi-static gravitational component, hence avoiding this problem.

2. Temperature drift and bias offset: The output of the ADXL335, among other factors, is also influenced by temperature, and it may even go unnoticed. In this instance, periodic calibration procedures, direct or indirect, and the application of temperature compensation curves are all strategies utilized to ensure that the orientation is accurate.
3. Non-orthogonality and scale factor mismatch: It is common for the specification tolerances to cause slight differences between the axes that are supposed to be orthogonal, thus necessitating matrix-based calibration to remedy the situation.
4. Resolution and quantization limits: The ADC resolution (usually 10–12 bits) has a limiting effect on the minimum tilt variation that can be detected; this range for well-calibrated systems is often between 0.5° to 1.0°.
5. Environmental coupling: The mechanical connection between the sensor and the surface being monitored is not ideal and therefore can either reduce or change the way tilt propagates. So, for the readings to be trustworthy, proper clamping and structural integration are obligatory.

The ADXL335 would deliver a static tilt resolution lesser than $\pm 0.5^{\circ}$ and an absolute accuracy of within $\pm 1.5^{\circ}$ after calibration in a lab setting [22]. On the other hand, outdoor or field sites with temperature changes, mechanical stress, and noise are usually considered can offer a practical accuracy of $\pm 2^{\circ}$, which is enough to notice initial slope displacements or barrier deformation before total collapse. To further strengthen reliability, the monitoring node may consist of the following [30–32]:

- Kalman filtering or complementary filtering for dynamic smoothing.
- Several redundant sensors, to ensure the validity of inclination readings.
- Both threshold-based and machine learning-based anomaly detection are used to pinpoint the angular deviations that are most likely associated with mass movement events.

The tilt angle's expression is directly derived from the gravitational acceleration vector projection as measured by a triaxial accelerometer. Using the inverse cosine and radian-to-degree conversion allows the sensor's inclination relative to any axis to be computed in real-time. This approach is the basis for the development of cost-effective IoT-based geotechnical monitoring systems that can detect ground instability phenomena early by carrying out continuous analysis of the angles.

3.1.3. LoRa Transceivers

Chirp Spread Spectrum (CSS) is a widely used long-range transmission protocol for low-power remote sensors [33]. It is a technology that uses radio frequency links that connect devices with each other as well as with gateways over kilometers, hence its low power consumption. The modulation of LoRa is based on CSS, and, together with the use of certain Spreading Factor (SF) and narrow channel bandwidths, it gives very high link robustness and range for disseminated networks [34]. LoRa technology is engineered for wind and solar resistance through low-bitrate transmission of small data packet sizes, and thus it is very efficient for a low-power sensor node. On the other hand, proliferation standards like Wi-Fi or Bluetooth will have much shorter coverage, which will still consume more energy than LoRa.

The regulatory standpoint gives a picture of LoRa as operating in the license-free ISM frequency bands, which are globally allocated for industrial, scientific, and medical use [33]. Thus, LoRa has become a reliable communication technology for spreading over a huge geographical area, along with the positive aspects of low cost, high-security links, and very small power consumption, although it cannot provide high throughput or meet stringent real-time requirements.

CSS that is overlaid by LoRa is a completely new method for data transmission, where pulses of chirps are used. The ch information is sent through chirp pulses, which are signals whose frequency is changed, erasing the time, i.e., either increasing (up-chirp) or decreasing (down-chirp) [34]. This method guarantees the highest possible immunity to interference and Doppler effects, and thereby, it will work perfectly for outside and shifting around areas. Two important factors influence the data rate for a specific LoRa link: the channel's bandwidth (BW) and the SF set on the sending unit. LoRa channels may have bandwidths of 125 kHz, 250 kHz, or 500 kHz, depending on the regional plan.

On the other hand, SF controls the chirp rate—the higher the SF, the longer the chirps, and, consequently, the lower the bit rate. Whenever SF is expanded by one, the time taken for the symbol to be recognized is also doubled, which effectively leads to the data rate being halved, and at the same time, the sensitivity of the receiver and the range of the link are improved. In conclusion, we can say the following:

- Lower SF → Faster transmission → Higher bit rate → Shorter range;
- Higher SF → Slower transmission → Improved sensitivity → Longer range.

SF7 to SF12 can be distinguished from each other, which means that when different SFs are used for transmitting at the same frequency, the signals will not interfere with one another [34]. This attribute is the main reason why LoRa networks have the advantage of not only being scalable but also consuming low energy. The nominal bit rate in LoRa modulation is given by Equation (9) [34]:

$$R_b = SF \times \frac{4}{(4+CR)} \times \frac{BW}{2^{SF}} \tag{9}$$

where

- R_b —nominal bit rate (bits/s).
- SF —spreading factor (7–12, depending on channel conditions).
- BW —modulation bandwidth (Hz).
- CR—coding rate (4/5, 4/6, 4/7 or 4/8).

The symbol period T_S represents the duration of one chirp and is calculated as [34]

$$T_S = \frac{2^{SF}}{BW} \tag{10}$$

ToA, the total time that a transmission occupies the channel depends on SF, BW, and payload length [34]:

$$ToA = T_{preamble} + T_{payload} \tag{11}$$

with

$$T_{preamble} = (n_{preamble} + 4.25) \cdot \frac{2^{SF}}{BW} \tag{12}$$

$$T_{payload} = [(8 + \max(N, 0)) \cdot (CR + 4)] \cdot \frac{2^{SF}}{BW} \tag{13}$$

where

$$N = \frac{8PL - 4SF + 28 + 16 - 20H}{4(SF - 2DE)} \tag{14}$$

and

- PL—payload size (bytes).
- H—header mode (0 = explicit, 1 = implicit).
- DE—low-data-rate optimization (1 for SF11/SF12, 0 otherwise).

It is true that lowering SF values or using shorter messages will lead to a reduction in the time taken for the transmission, and, thus, the energy consumed by the node will also be lower. The energy required for one transmission is [34]

$$E = P_{tx} \times ToA \tag{15}$$

In battery time, high SF poses much more transmission time. Considering possible retransmissions, if P_{loss} denotes the packet loss rate, the total energy expenditure becomes

$$E_{total} = E \times (1 + P_{loss}) \tag{16}$$

Minimizing collisions and interference reduces P_{loss}, improving the network's overall energy efficiency.

First, the field in every LoRa frame is a preamble, which acts as a synchronizing signal for both the transmitter and the receiver. The preamble consists of several unchanging up-chirps, two more up-chirps that carry the synchronization word, and about 2.25 down-chirps for frame delimitation [35,36]. The preamble duration can range from 10.25 to 65,539.25 symbols, depending on the configuration. The following fields form the LoRa physical frame:

- Header and Header Cyclic Redundancy Check (CRC): Define payload size and coding rate, occupying 2 bytes.
- Payload: Sensor data or application information (e.g., latitude, longitude, Inclination on X-axis (degrees), inclination on Y-axis (degrees), inclination on Z-axis (degrees); we used 35 bytes.
- CRC Payload (optional): Used for integrity verification.

An example of payload layout used in the experimental setup was:

$$\text{Lat} \mid \text{Lng} \mid \text{INC\_X} \mid \text{INC\_Y} \mid \text{INC\_Z}$$

The Received Signal Strength Indicator (RSSI) is a measurement of the received signal strength expressed in dBm [36,37]. The factors determining RSSI are transmitter output power, free-space loss, antenna gain, and obstructions in the environment. The Signal-to-Noise Ratio (SNR) measures the relation between signal power and noise power:

$$SNR_{dB} = P_{RX(dBm)} - P_{NOISE(dBm)} \tag{17}$$

A good SNR indicates that the signal is well above the noise floor, thus allowing for proper demodulation. Demodulation, even below the noise level, is one of the strengths of LoRa, making its range very wide. By using standard LoRa settings (14 dBm Tx, -130 dBm Rx, 1.5 dBi antenna), the theoretical distance in an unobstructed view might be over 10 km, but the actual performance will depend on the terrain.

In this case, two LoRa transceivers were used for communication between the node and the gateway, with each working at 868 MHz, and fully capable of handling the LoRa spread-spectrum modulation and 3.3 V I/O voltage.

In summary, LoRa can offer long-distance communication, very low power consumption, and good signal processing by using its CSS modulation and adjustable characteristics (SF, BW, and Coding Rate (CR)). The careful choice of these parameters, most of all the spreading factor, results in an ideal combination of energy consumption, coverage, and data rate, thus making LoRa a highly suitable option for sensor networks in environmental and industrial monitoring areas.

3.1.4. Power Supply

To power the LilyGo module, the XTAR 18650 [38] 2600 mAh battery (with protection) was selected. The technical specifications are presented in Table 6.

Table 6. Technical specifications of the battery (adapted from [37]).

Parameter	Value/Details
Battery chemistry	Li-ion
Voltage	3.6 V
Typ. capacity	2600 mAh (typical)/2550 mAh (min)
Discharge current—A	5.20
Battery version	Button top
Dimensions	68.5 mm (height) × 18.4 mm (diameter)

3.1.5. Monitoring System—Dashboard

An HTML dashboard was developed that receives data from Gateway through a Python version 3.11.0 script. This script reads information from the serial port (sent by the Gateway) and transmits it to the dashboard. The main objective is to enable remote access to this data from any location, and it is also responsible for issuing alerts that notify users about any anomalies detected. To make the localhost publicly accessible, Ngrok [39] was used. However, since the free version was employed, there is a limitation: whenever the service is restarted, a new random link is generated. As this is a laboratory experience, this limitation does not pose a significant issue.

3.2. Algorithms Developed

In this section, we present the algorithms developed for the IoT detection node and for the gateway.

The microcontrollers were programmed using the Arduino IDE, chosen for its versatility and widespread adoption in embedded projects. The Arduino IDE, with its vast ecosystem of libraries, streamlines the development and testing process, ensuring optimized and reliable code. The language used in the program is C++. Figure 2 shows the IoT detection node flowchart.

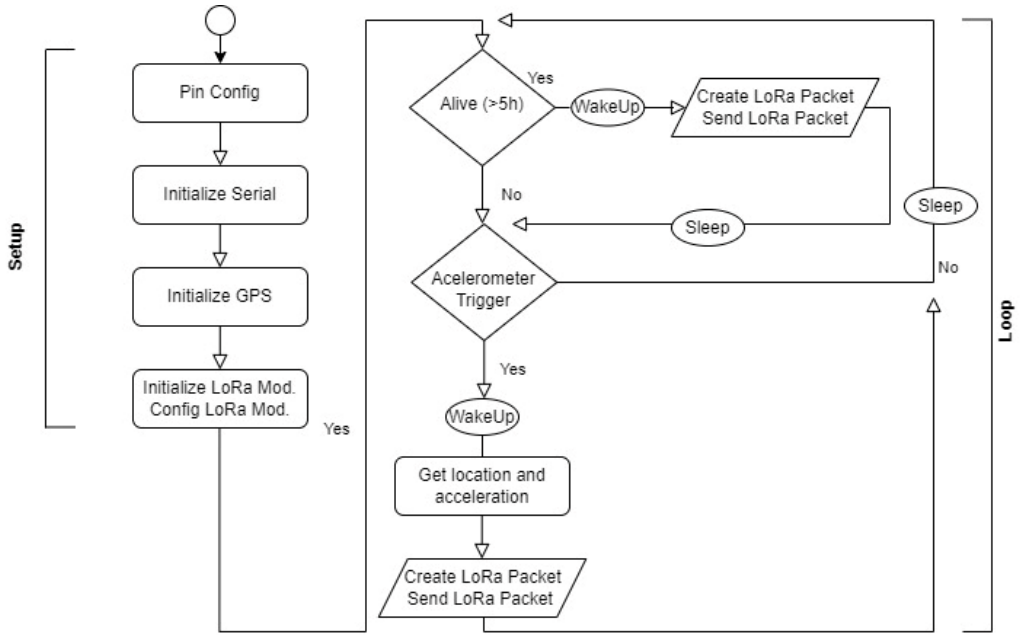

Figure 2. IoT detection node flowchart.

Figure 3 shows the gateway flowchart.

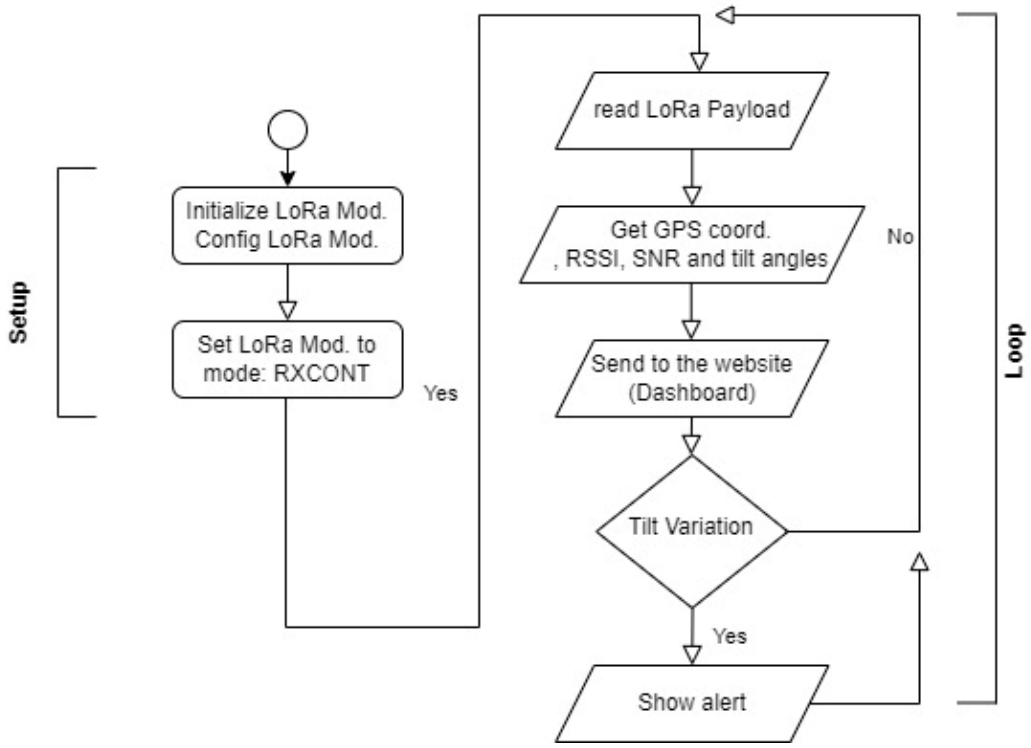

Figure 3. Gateway flowchart.

Algorithm 1 represents the firmware developed for the IoT detection node, and Algorithm 2 represents the firmware developed for the gateway.

Algorithm 1: IoT detection node

```
BEGIN
  INITIALIZE serial interfaces (USB, GPS)
  INITIALIZE LoRa radio with frequency, SF, BW, CR
  INITIALIZE ADXL335 accelerometer input pins
  REMOVE tilt values saved in power resume memory

  LOOP once per wake cycle:
      READ GPS data from NEO-6M
      COMPUTE average ADC readings (X, Y, Z)
      CONVERT ADC values to acceleration (g)
      CALCULATE tilt angles INC_X, INC_Y, INC_Z
      IF (tilt values changed OR timer elapsed):
          FORMAT message:
              "LAT:<lat>,LNG:<lng>,INC_X:<x>,INC_Y:<y>,INC_Z:<z>"
          TRANSMIT packet via LoRa
          STORE last tilt and GPS values in real-time clock memory
      ENDIF
      ENTER deep sleep for predefined interval
  END LOOP
END
```

Algorithm 2: Gateway

```
BEGIN
  // Stage 1: LoRa Gateway Receiver
  INITIALIZE Serial(115200)
  INITIALIZE LoRa transceiver with frequency, SF, BW, CR, and CRC enabled
  LOOP continuously:
      IF LoRa packet received THEN
          payload: LoRa.readPacket()
          rssi: LoRa.packetRssi()
          snr: LoRa.packetSnr()
          PRINT "Received packet '<payload>' with RSSI <rssi> and SNR <snr>"
      ENDIF
  END LOOP
  // Stage 2: Data Bridge and Processing Server (Python/Flask-SocketIO)
  CREATE Flask web server
  INITIALIZE SocketIO module for real-time communication
  TRY open serial port (e.g., COM5, 115,200 baud)
  IF successful THEN
      START background thread read_serial:
          LOOP indefinitely:
              IF serial data available THEN
                  serial.readline().decode().strip()
                  EMIT SocketIO event 'novo_dado' with {"mensagem": line}
              ENDIF
      END LOOP
  ENDIF
  DEFINE web route "/" → render HTML dashboard (index.html)
  START SocketIO server at host 0.0.0.0, port 5000

  // Stage 3: Real-Time Web Dashboard (HTML and JavaScript)
  ON browser page load:
      INITIALIZE Leaflet map centered at default coordinates
      INITIALIZE Chart.js plots for signal metrics (RSSI, SNR)
      INITIALIZE Chart.js plots for inclination metrics (INC_X, INC_Y, INC_Z)
      CONNECT to Socket.IO server
  ON event 'new_data' received:
      current time
      UPDATE "last update" indicator with now
      // Parse MCU log line:
      MATCH "Received packet '(.*)' with RSSI ([\-0–9.]+) and SNR ([\-0–9.]+)"
      IF match valid THEN
          packet: match.group(1)
          rssi: float(match.group(2))
          snr: float(match.group(3))
          PARSE packet fields
"LAT:<val>,LNG:<val>,INC_X:<val>,INC_Y:<val>,INC_Z:<val>"
          UPDATE map marker and coordinates display
```

Algorithm 2: Cont.

```
            APPEND values to recent readings list
            UPDATE charts for RSSI/SNR and tilt (INC_X, INC_Y, INC_Z)
            IF |INC_Y| > threshold THEN
                DISPLAY alert (e.g., barrier movement)
            ELSE
                HIDE alert
            ENDIF
        ENDIF
    // Stage 4: Data Flow Summary
    /* LoRa Node (sensor) send to Gateway (Arduino), after via Serial Port send to
Flask/SocketIO Server and display in Web Dashboard (Map, Charts and Alerts) */
END
```

The algorithm that is suggested creates a direct and uninterrupted flow of data throughout the entire process between the pole sensor node, the gateway, and the visualization interface. The Arduino-based gateway obtains LoRa packets from the remote node, decodes the payload, and then outputs the complete message through its serial interface in the first phase. This complete message contains not only sensor information but also related signal parameters like RSSI and SNR. A Python application based on the Flask-SocketIO framework handles the second phase, continuously monitoring the serial port, parsing each received line, and hence emitting the processed content as real-time WebSocket events immediately. The HTML dashboard captures these events in the third phase, where the GPS coordinates and inclination data are dynamically extracted and displayed. After that, the web interface updates a Leaflet map to represent the current position of the node and refreshes Chart.js visualizations showing signal strength and angular variations. Also, it activates visual alerts whenever the measured tilt goes beyond the specified thresholds. Thus, all these activities together form a smooth and self-sufficient IoT data pipeline that allows for the automatic acquisition, transfer, and visualization of environmental and structural information, from the LoRa field node to the online monitoring dashboard via the gateway.

4. Results

In Section 4.1, we describe experiment scenarios and the possible adaptation of different scenarios and situations. In Sections 4.2 and 4.3, experimental tests were made for the accelerometer and LoRa radio. In Section 4.4, we present a dashboard website that shows the data from our experience, and finally, in Section 4.5, we write about the energy consumption of the IoT node.

All the trials have been performed on even plain surfaces with regulated platform movements, which, however, do not reflect the actual situations of geotechnical instability. Thus, the outcome should be taken as preliminary proof of technology conception.

4.1. Experiment Scenarios

Figure 4 depicts an entire system design for detecting landslide potential risk by means of an IoT node with LoRa service. The IoT detection node is located on the slope surface on the left side of the image. In this study, real topographic data from the Peneda–Gerês mountain range region (North Portugal, specifically along the N304 road, at coordinates 41.7365° N, −8.1678° W) were used to estimate the slope inclination first. From the two reference topographic points, one at 440 m and the other at 625 m altitude, a horizontal distance of 326.07 m was measured between them. The usual slope Equation (18) was then applied:

$$i(\%) = \frac{\Delta h}{d} \times 100 \tag{18}$$

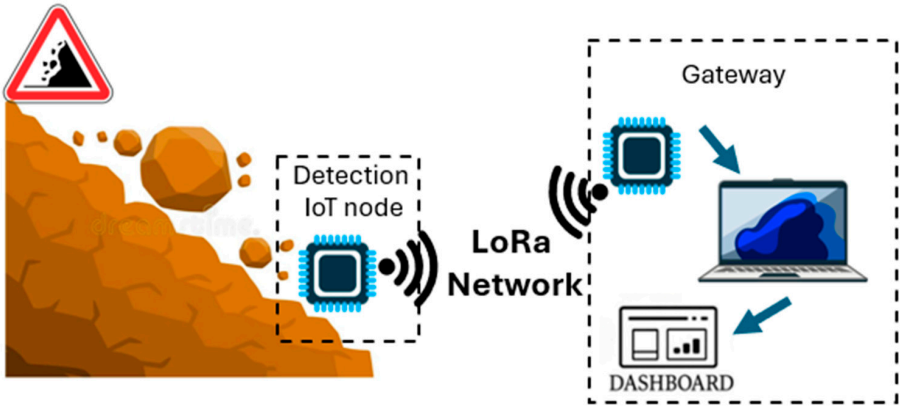

Figure 4. Block diagram to test our experience.

In this situation, the calculated slope equals 56.73%. Hence, the IoT node will be gradually set up at this primary angle. The angle on the *X*-axis was evaluated live by utilizing the accelerometer-based estimation method specified in Equation (8). This equation enables the node to constantly determine the angle of inclination in degrees. The system was set up to regard 56.73° as the reference angle of the terrain. Whenever deviations exceeding ±2° are noticed (i.e., values more than 58.73° or less than 54.73°), alerts are set off. This tolerance range was stipulated to recognize the soil mass movements that could be dangerous in terms of landslide increments, with the onset of soil movement of this kind being the situation in early landslides. The inclined plane values that were calculated are sent through the LoRa network to a distant gateway, which transmits the information to a back-end dashboard. This dashboard (in Section 4.4) provides the ability to perform live monitoring, view the angle changes, and send alarm signals to operators or authorities in case critical deviations are reported. Ultimately, the reason behind this method is that the experimental system can be easily modified to any place on Earth just by setting the reference slope according to actual topographic conditions. In the case of a new site being investigated, it suffices to calculate the local reference slope through Equation (8) (which considers the specific altitude variation and horizontal distance of that terrain). This means that the same IoT system can be adapted to different slopes without changing the sensing equipment, just by altering the reference angle parameter and the alert thresholds in accordance.

We developed physical prototypes for this experiment, which consist of two main modules: the gateway (Figure 5a) and the IoT detection node (Figure 5b).

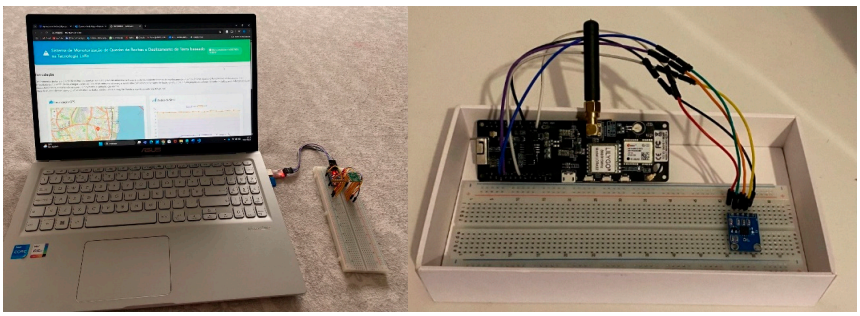

(**a**) (**b**)

Figure 5. Developed prototypes: (**a**) gateway on the left side and (**b**) IoT detection node on the right side.

Figure 6 shows a site accessed by another device, connected to the gateway (using a Wi-Fi network).

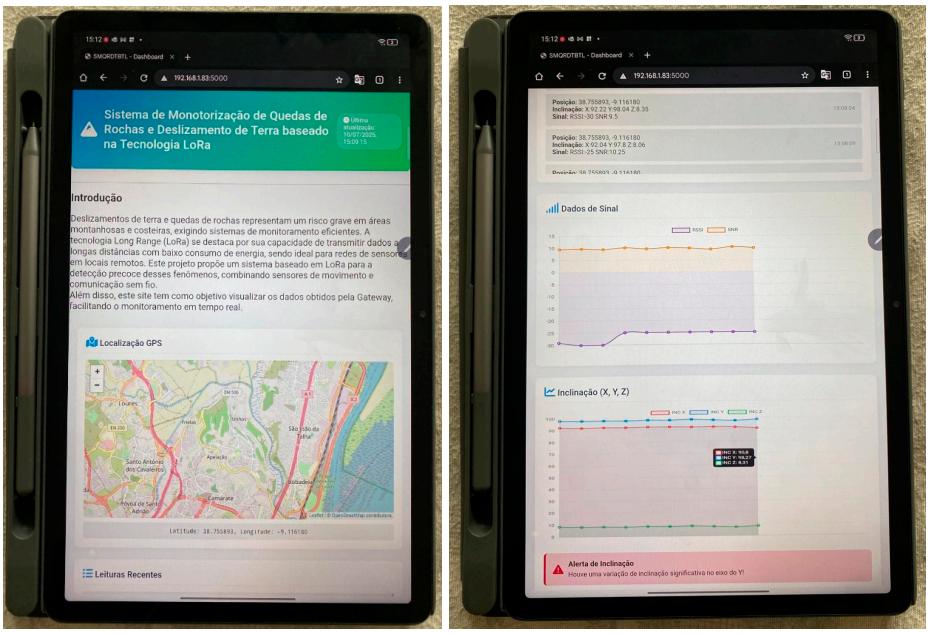

Figure 6. Site accessed via tablet.

4.2. Accelerometer Tests

To validate the proposed method of slope danger detection, tests were conducted in the laboratory using a static IoT node equipped with a triaxial accelerometer as the main tool. The node was placed on a mechanical support that could change its angle in a controlled and repeatable manner. The main aim of these early tests was to generate tiny angular deviations around the reference slope of 56.73° to check the sensor's capability to recognize deviations equal to or greater than the $\pm 2^\circ$ limit, which is the set threshold for triggering alerts. For this trial, a three-hour continuous data acquisition (total of 10,799 s, one sample per second) was performed. The platform was periodically subjected to small controlled manual perturbations (increases of $+1^\circ$ to $+3^\circ$ and decreases of -1° to -3°) to mimic micro-movements associated with the early stage of soil displacement.

The data from the accelerometers that were recorded during the experiments were processed according to expression (8), which transformed the raw acceleration components (a_x, a_y, a_z) into an angle of inclination for the X-axis. The graphical analysis (inclination vs. time) resulting from this process shows that the system keeps stable readings for the case of constant inclination and accurately shows angular variation when the support is slightly rotated to simulate micro-displacements. At the same time, through the test sequences, artificial "micro-events" were introduced, and the graphs clearly show that deviations above $+2^\circ$ and below -2° from the reference immediately cross the decision boundary. This supports the notion that the algorithm relying on the accelerometer and expression (8) indeed offers a straightforward yet extremely reliable mechanism for the detection of potentially adverse slope variations.

The oscillation in the X-axis acceleration (Figure 7) is quite subtle, oscillating around a baseline of nearly 0 G, yet the several perturbation events are very clear through the sudden spikes between about -0.45 G and $+0.40$ G. The height of these spikes is equal to that of the short, impulsive angular changes carried out by hand.

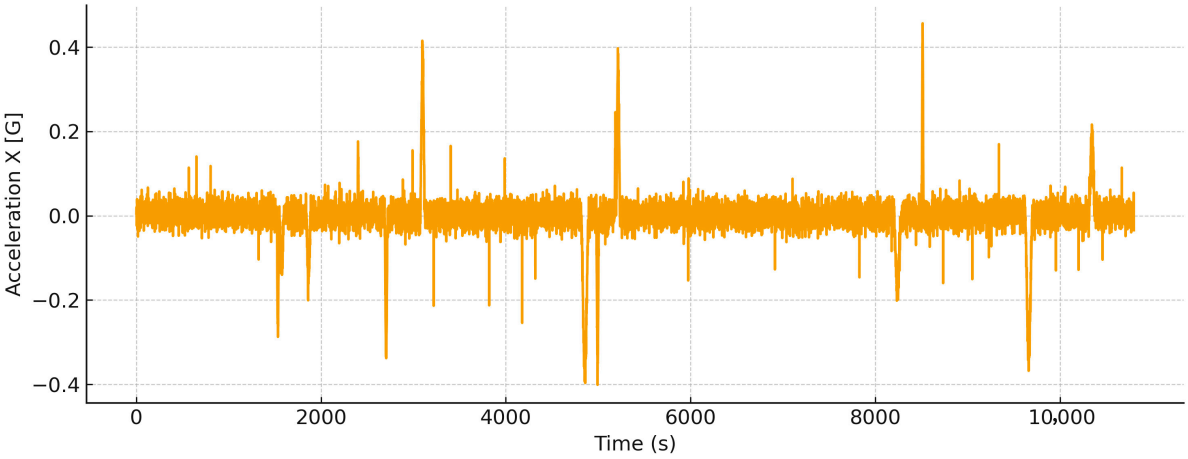

Figure 7. *X*-axis acceleration vs. time.

The *Y*-axis traces (Figure 8) a diagram like the *X*-axis. The noise of the baseline is limited to a very small fluctuation around 0 G, while the caused events generate shifts between approximately −0.38 G and +0.28 G. Thus, it is validated that platform rotations create simultaneous effects on both X and Y axes.

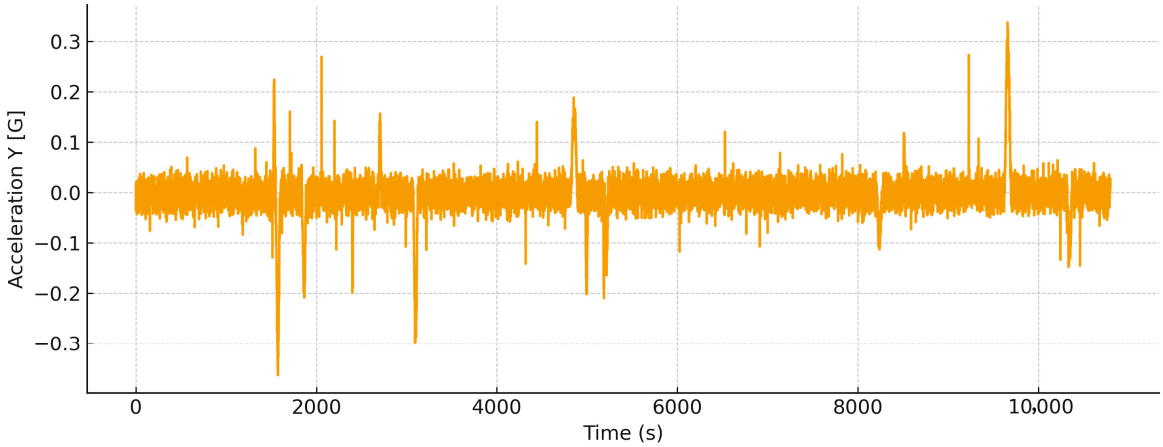

Figure 8. *Y*-axis acceleration vs. time.

The *Z*-axis (Figure 9) is demonstrating readings with a mean value of 1 G, which matches the force of gravity. A very short-time phenomenon below 0.8 G and above 1.2 G serves as confirmation that during tilting, the angular coupling occurs between axes.

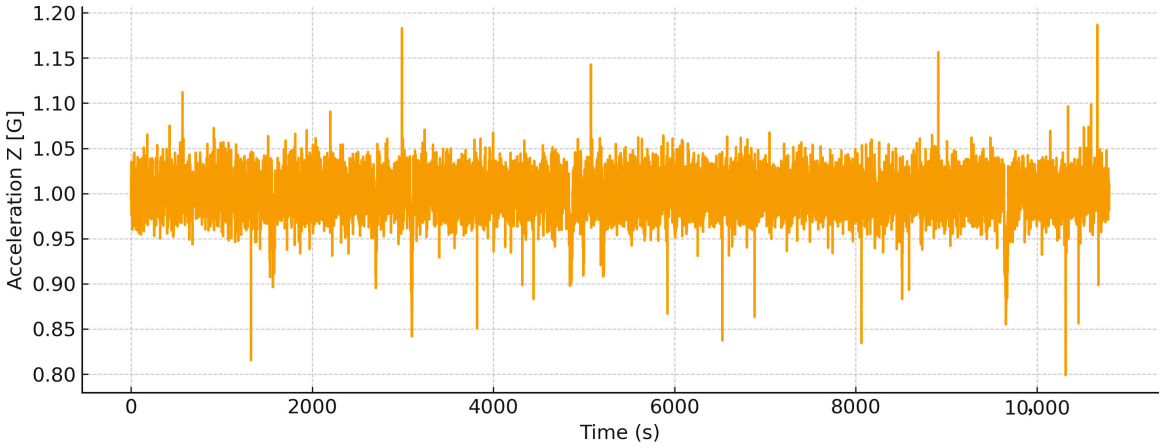

Figure 9. *Z*-axis acceleration vs. time.

Figure 10 presents the computed roll angle, where deviations above ±2° correspond to induced perturbations used to validate the detection threshold.

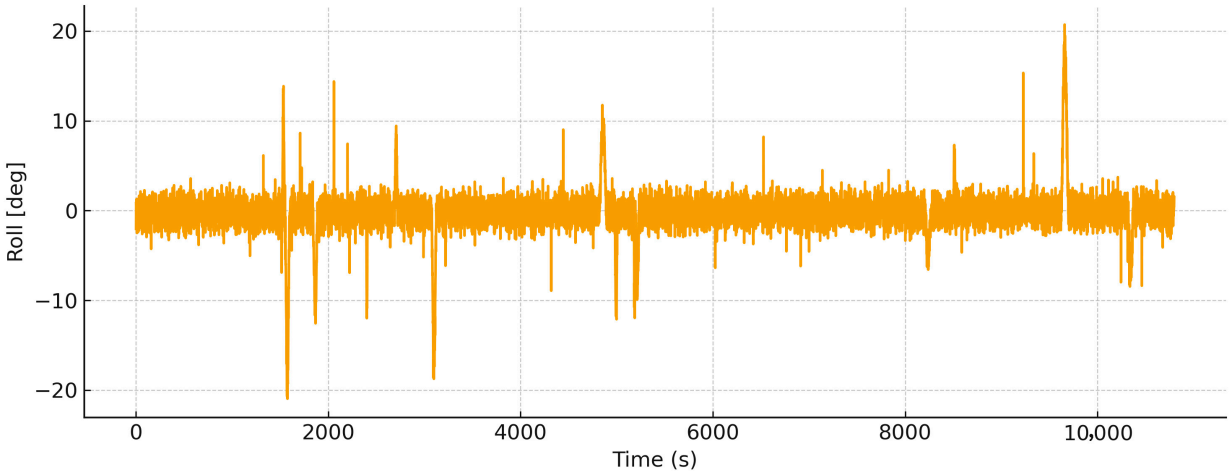

Figure 10. Roll vs. time, adding movement events.

Pitch (Figure 11) has more pronounced peaks (above 20°) and negative dips as low as −25°. To test the system's behavior and performance near saturation, larger rotations were deliberately produced.

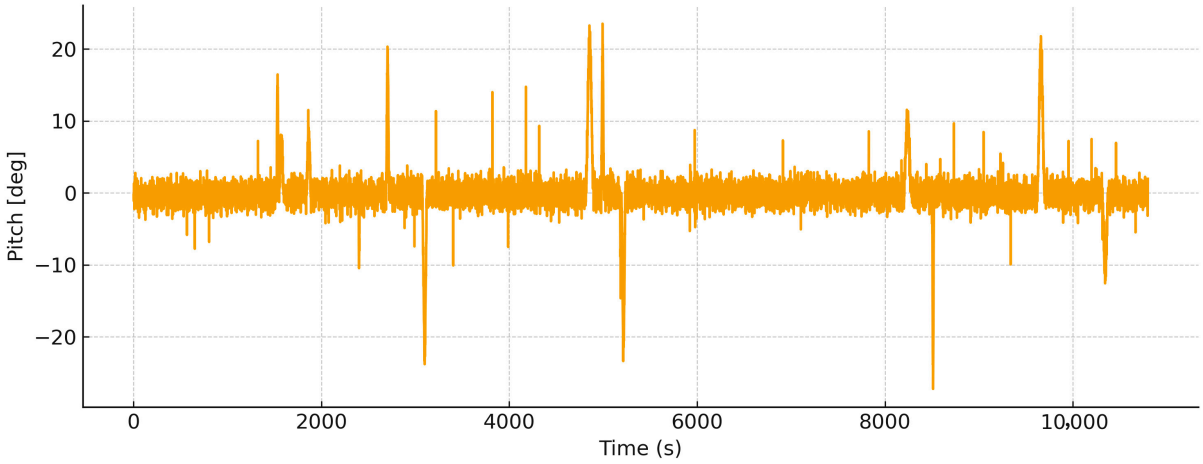

Figure 11. Pitch vs. time.

This representation of angles, see Figure 12, indicates the effects of tilting on all axes, with peaks above 30° being induced. This is a good phenomenon because landslide precursors usually appear in the form of coupled multi-axis micro-displacements.

In summary, the bench tests proved the working principle: small angular deviations were monitored nearly in real time, and the attribution limit of ±2° was adequate to tell apart normal background oscillation (under ±2°) and critical displacement (over ±2°). The results, though gained in a controlled environment, were very conclusive for the proposed technique's viability. The next phase is to position the node right where the action is, with the same computation technique, but by adjusting the initial reference angle to each specific terrain where the setup is located. This plan allows total portability of the experimental setup, as the only variable that changes from one place to another is the reference slope derived from the topographical data of the area being studied.

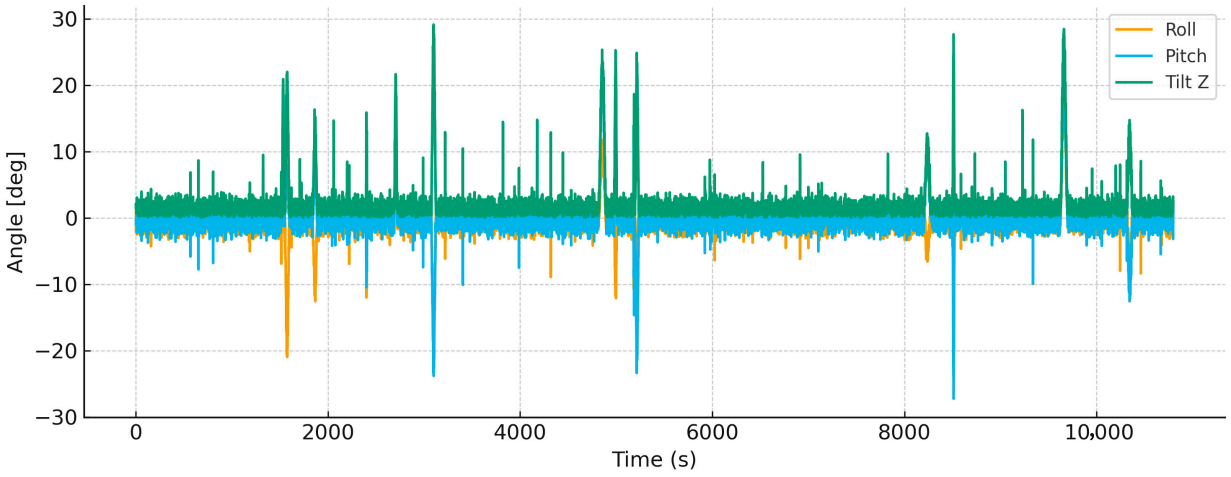

Figure 12. Angles vs. time.

4.3. LoRa Radio Tests

Outdoor practical tests were conducted between the IoT detection node and the gateway, with BW fixed at 125 kHz and CR 4/5 with a 35 B payload, while varying SF (7 to 12), transmission power (6 and 14 dBm), and distance (400 to 2000 m). The objective was to evaluate how these parameters impact connection stability, packet loss, and energy efficiency, seeking the best configuration for LoRa networks in different scenarios. The results show the trade-offs between range, consumption, and robustness, helping to select optimal parameters for real-world applications. Figure 13 shows the location under conditions with and without line of sight where the tests were conducted, and Figures 14–17 present the results obtained at the Gateway.

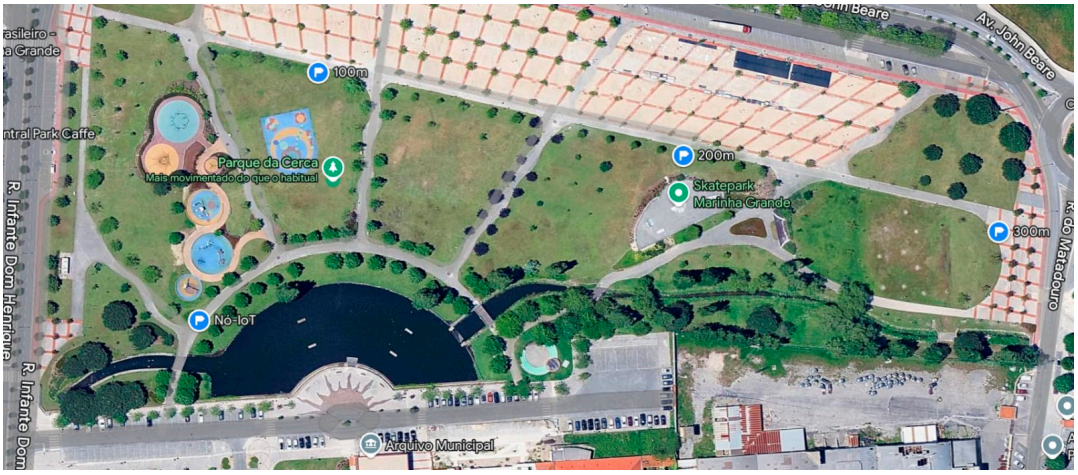

Figure 13. Radio test location.

The measurements were performed in an open public park in Marinha Grande, Portugal (refer to Figure 13). The chosen area provides unobstructed long-range segments that ensure stable visibility between the transmitter and the receiving node. Nonetheless, some sections of the path did include short sections without line-of-sight conditions, which were purposely introduced by the presence of tree clusters, pedestrian infrastructure, and temporary buildings or metal structures obstructing the view around the park's perimeter. The whole measurement campaign covered distances ranging from 400 m to 2000 m, and the separation between the nodes was increased step by step to assess the corresponding effect on signal strength and link quality in realistic outdoor mixed with and without line-of-sight scenarios.

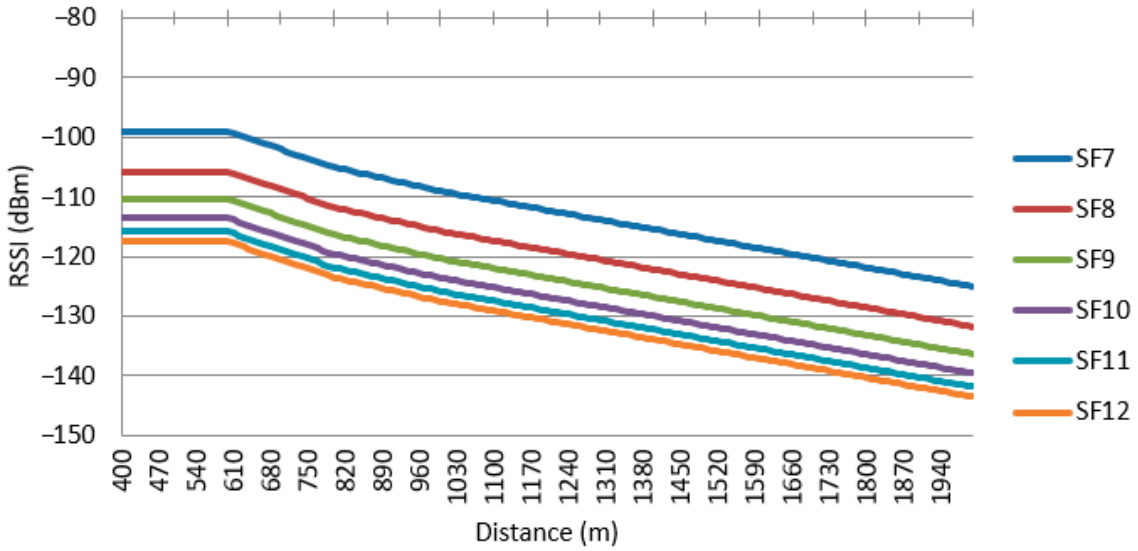

Figure 14. RSSI on the gateway side with power transmission of 6 dBm.

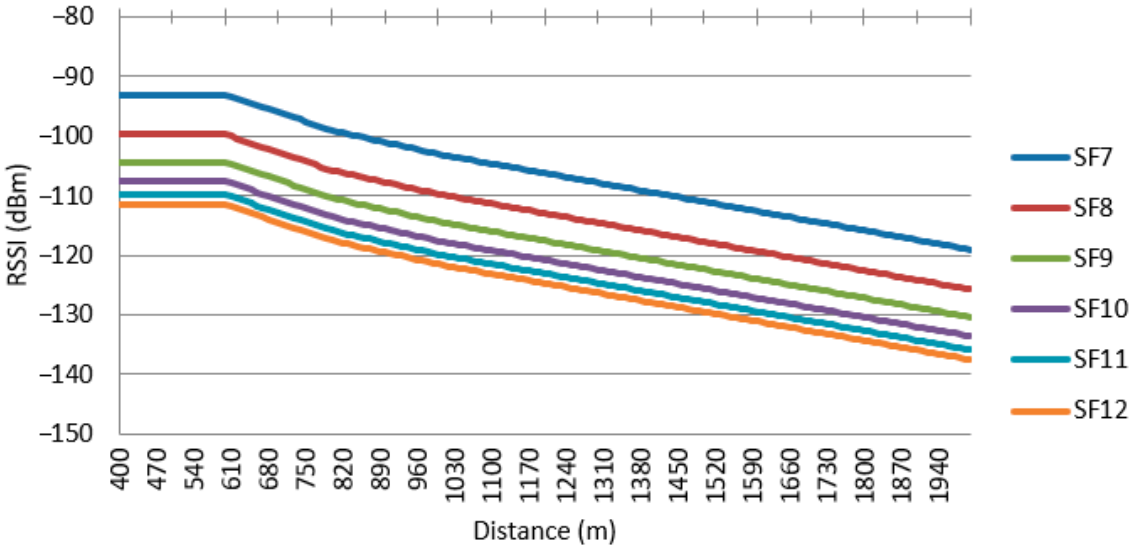

Figure 15. RSSI on the gateway side with power transmission of 14 dBm.

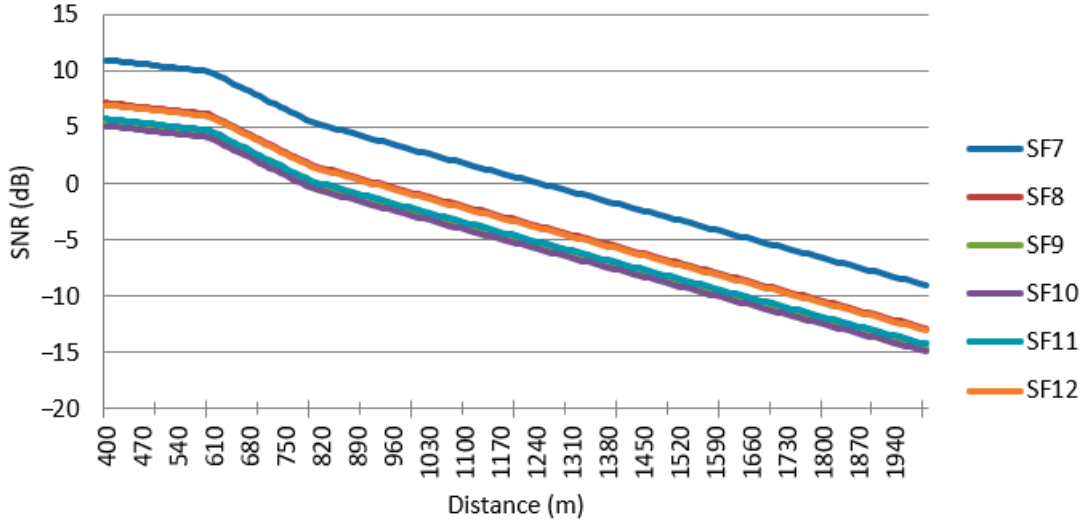

Figure 16. SNR on the gateway side with power transmission of 6 dBm.

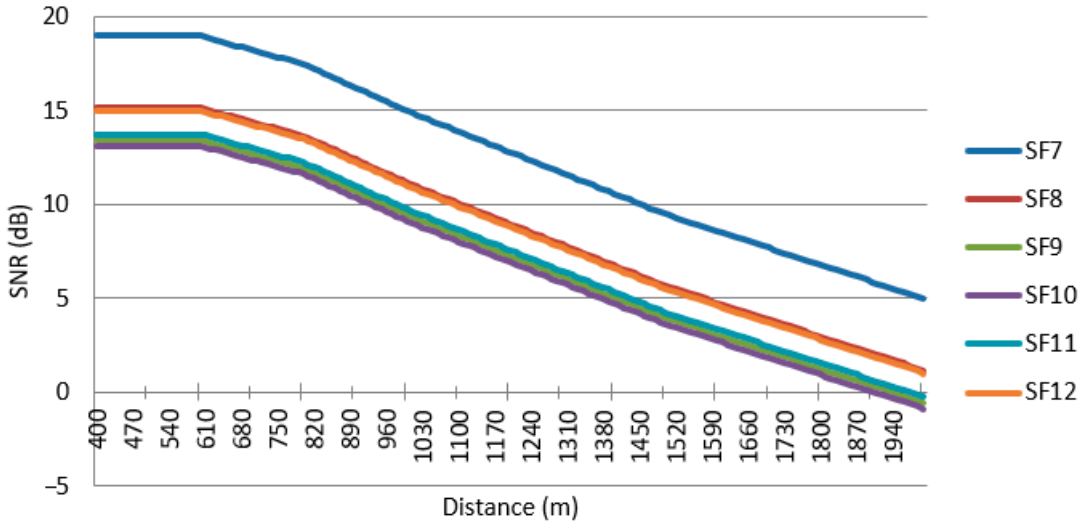

Figure 17. SNR on the gateway side with power transmission of 14 dBm.

Figure 14 depicts the progression of RSSI with distance at an output power of 6 dBm. It is possible to see that the loss behavior is typical and of a progressive nature as the distance increases. SF7, which is the lowest of the four options, has the highest RSSI in the beginning, but the gap to other SFs is reduced over time. The higher SFs have lower levels at the start, but their slopes are very much alike throughout the path. All in all, the curve set presents the anticipated LoRa envelope at low power, in an outdoor scenario where mixed with and without line-of-sight conditions are applied.

As in Figure 14, Figure 15 illustrates the same situation, but now a power increase of 14 dBm is applied. The fact that the curves of all values have been raised shows the direct gain in link budget that comes with a power increase. The qualitative difference between SF7 and SF12 still holds, but the higher power provides all SFs with easier reception over nearly the whole distance.

Figure 16 illustrates the SNR at 6 dBm. Initially, SF7 has a much greater SNR for close distances, but it declines quickly. Increased SFs then trace more compressed paths and enter the 0 dB area at roughly the same time as or just after SF7. The area of negative SNR at greater distances denotes the anticipated deterioration caused by the combination of propagation loss, multipath dispersion, and without line-of-sight segments along the route.

At 14 dBm (refer to Figure 17), the starting SNR for every SF is more than that of the others. SF7 is still the best option for short distances in this case, but the difference between higher SFs and SF7 increases earlier as the distance grows. SF10–12 keep the SNR in the usable range for a longer distance, thereby confirming that the pairing of higher power and SF is still the best for real-world situations of poor propagation.

Graphs are quite explicit in pointing out the arrangement trade-offs between range, SF, and link performance. In the case of the park chosen for the field experiments, which has occasional obstructions, it was the combination of "high SF + moderate power" that proved to be the most stable and efficient compromise for the long uplinks while guaranteeing high energy autonomy, just the critical requirement for monitoring remote and unstable slopes.

4.4. Dashboard

As previously mentioned, a current inclination of 56.73 degrees was identified. The system was configured so that the gateway responsible for data processing issues an alert whenever it detects a variation greater than ±2 degrees relative to this reference value, if the inclination exceeds 58.73 degrees or falls below 54.73 degrees. This safety margin was established to capture significant movements that may indicate risks, such as landslides or

ground instability. The IoT detection node sends readings based on the accelerometer's trigger to the gateway, which compares the received data with the baseline value and triggers an alert protocol, which may include real-time notifications. For testing purposes, only the inclination value of the *Y*-axis was considered; Figure 18 shows the results.

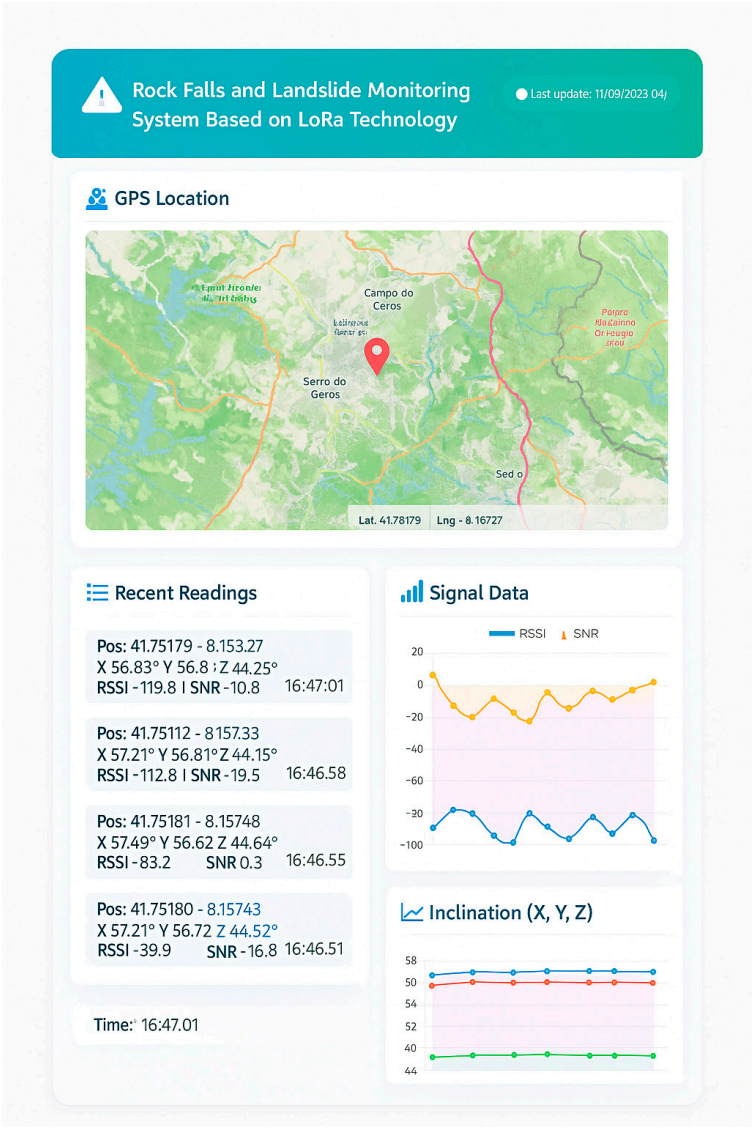

Figure 18. Dashboard with the results.

The web dashboard shown in Figure 18 was developed for real-time monitoring of data collected by sensor nodes. The geographical location (GPS map with the node position), the instantaneous RSSI, and SNR values received at the gateway, along with the inclination in each of the axes (X, Y, Z) calculated from the Micro-Electro-Mechanical Systems accelerometer, are integrated in a single panel through the interface. This combination of information allows for direct correlation of radio performance with the mechanical condition of the sensor by providing a complete operational view of the state of the system in the field.

A list of recent readings is displayed in the lower part of the dashboard, where each timestamp shows the position, tilt, and related signal values. The users will see whether the tilt algorithm has detected the motion consistently over time, and the LoRa connection has been stable even in an environment with obstructions and multipath. In practical terms, the interface is the last link in the system's functional chain, and it shows that the proposed

solution is not only technically feasible but also directly usable for operational monitoring in real geological risk scenarios.

4.5. Consumption

Nominal consumption refers to the amount of electrical energy consumed by each system component during standard operation. This subsection addresses the nominal consumption of the IoT detection node, since it operates on battery power, and its autonomy depends directly on the energy efficiency of the integrated devices. Table 7 presents the nominal consumption values for each component listed in the system:

Table 7. Nominal consumption.

Component	Nominal Consumption
Motion Sensor (ADXL335)	350 µA
GPS Module (NEO-6M)	22 µA
Microcontroller (ESP32)	39 mA
LoRa Transmitter (SX1276)	120 mA (1% of communication time)

According to Table 6, considering the system's maximum nominal consumption, the battery duration would be (2600 mAh)/(159.372 mA) $\approx$ 16.3 h. However, this calculation represents the worst-case scenario, as it assumes continuous operation and does not account for the intermittent nature of LoRa transmissions. The system operates in active and sleep cycles, which allows for a significant reduction in average power consumption. By using low-power mode (deep sleep) and turning off components when not in use, power consumption can be significantly reduced. Knowing that in deep sleep mode the ESP32 consumes 10 µA and the LoRa transmitter consumes 0.2 µA, and that we can turn off the motion sensor when not in use, the new battery duration would be approximately 13.5 years. It is important to note that in practice, batteries have self-discharge and losses, so the actual duration will be shorter.

5. Conclusions and Future Work

The system developed is a proof-of-concept prototype to evaluate, from an experimental point of view, the possibility of using a LoRa solution for an early warning against slope movements.

The study proved the fulfillment of a LoRa-based monitoring system that could detect the smallest slope variants. To confirm the technique of determining slope from triaxial accelerations, the laboratory tests were performed first and then followed by outdoor tests in urban settings with and without line-of-sight propagation, where distances of 400 m to 2000 m were recorded. The calibrated Micro-Electro-Mechanical Systems accelerometer identified more than $\pm 2^{\circ}$ changes in relation to the ground reference value, thus permitting the detection of micro-displacements. The radio part of the study revealed that the use of moderate SF (SF8) settings combined with a 125 kHz bandwidth yielded the best tradeoff between the distance signal and power drain, while keeping SNR levels usable even in situations with obstacles.

Moreover, there was a real-time monitoring web application that was built, allowing the display of GPS position, the tilt in the three axes, and the radio performance (RSSI and SNR) right from the gateway's data collection. The dashboard demonstrates not only the system's operability but also its maturity, as it represents the whole process in an integrated manner: firstly, sensor (to collect data) data, sent via the LoRa network to the LoRa gateway, where there are two possibilities for visualization: local or Internet.

More field tests are required in future work, for the system in their operating environment and climactic conditions, in different types of terrain performance verification.

In the future, we will add solar energy harvesting to the system, which will make the system last for several months without recharging in the field, and inputting machine learning to differentiate between actual movements and non-structural vibrations is among the plans. Moreover, there will be an extension of experimental campaigns throughout the country in areas with different morphologies for the purpose of adaptability validation to different terrains. Future work will extend field testing to different terrain types, evaluate energy-harvesting options, and integrate advanced filtering or machine-learning techniques for improved event classification.

Author Contributions: Conceptualization, L.M.P. and I.V.; methodology, L.M.P.; software, I.V.; validation, L.M.P.; formal analysis, L.M.P. and I.V.; investigation, L.M.P. and I.V.; resources, L.M.P.; data curation, L.M.P. and I.V.; writing—original draft preparation, I.V.; writing—review and editing, L.M.P. and I.V.; visualization, I.V.; supervision, L.M.P. All authors have read and agreed to the published version of the manuscript.

Funding: This research received no external funding.

Data Availability Statement: Data are contained within the article.

Conflicts of Interest: The authors declare no conflicts of interest.

Abbreviations

The following abbreviations are used in this manuscript:

ADC	Analog-to-Digital Converter
AWSs	Amazon Web Services
BLE	Bluetooth Low Energy
BW	Bandwidth
CRC	Cyclic Redundancy Check
CR	Coding Rate
CSS	Chirp Spread Spectrum
EEPROM	Electrically Erasable Programmable Read-Only Memory
GNSS	Global Navigation Satellite System
GPS	Global Positioning System
HTML	HyperText Markup Language
I2C	Inter-Integrated Circuit
IoT	Internet of Things
LoRa	Long Range
LoRaWAN	Long-Range Wide-Area Network
MCU	Microcontroller Unit
NMEA	National Marine Electronics Association
RAM	Random Access Memory
ROM	Read-Only Memory
RSSI	Received Signal Strength Indicator
SF	Spreading Factor
SNR	Signal-to-Noise Ratio
SPI	Serial Peripheral Interface
SRAM	Static Random Access Memory
ToA	Time-on-Air
TTN	The Things Network
UART	Universal Asynchronous Receiver/Transmitter
USB	Universal Serial Bus

References

1. Autoridade Nacional de Emergência e Proteção Civil. Avaliação Nacional de Risco—Revisão 2023. Available online: https://prociv.gov.pt/media/h4fgmxul/anr2023_revis%C3%A3o_ultima.pdf (accessed on 13 March 2025).
2. EuroNews. Deslizamentos de Terras na Serra da Estrela. Available online: https://pt.euronews.com/2022/09/13/deslizamentos-de-terras-na-serra-da-estrela (accessed on 13 March 2025).
3. AiKo. LoRa Technology Overview. Available online: https://aiko.digital/lora/ (accessed on 13 March 2025).
4. Gokhale, P.; Bhat, O.; Bhat, S. Introduction to IoT. *Int. Adv. Res. J. Sci. Eng. Technol.* **2018**, *5*, 41–44.
5. Farooq, M.U.; Waseem, M.; Mazhar, S.; Khairi, A.; Kamal, T. A Review on Internet of Things (IoT). *Int. J. Comput. Appl.* **2015**, *113*, 1–7. [CrossRef]
6. Statista. IoT Connected Devices Worldwide 2019–2030. Available online: https://www.statista.com/statistics/1183457/iot-connected-devices-worldwide/ (accessed on 9 May 2025).
7. Mohammadi, M.; Al-Fuqaha, A.; Sorour, S.; Guizani, M. Deep Learning for IoT Big Data and Streaming Analytics: A Survey. *IEEE Commun. Surv. Tutor.* **2018**, *20*, 2923–2960. [CrossRef]
8. Sagiroglu, S.; Sinanc, D. Big Data: A Review. In Proceedings of the 2013 International Conference on Collaboration Technol-ogies and Systems (CTS), San Diego, CA, USA, 20–24 May 2013; pp. 42–47. [CrossRef]
9. Ragnoli, M.; Scarsella, M.; Leoni, A.; Ferri, G.; Stornelli, V. Wireless Sensor Network-Based Rockfall and Landslide Monitoring Systems: A Review. *Sensors* **2023**, *23*, 7278. [CrossRef] [PubMed]
10. Ragnoli, M.; Leoni, A.; Barile, G.; Ferri, G.; Stornelli, V. LoRa-Based Wireless Sensors Network for Rockfall and Landslide Monitoring: A Case Study in Pantelleria Island with Portable LoRaWAN Access. *J. Low Power Electron. Appl.* **2022**, *12*, 47. [CrossRef]
11. Muladi, M.; Amarda, S.Y.; Mahamad, A.K.; Prasetyo, S.D.; Harsito, C. LoRaWAN and IoT-Based Landslide Early Warning System. In *Advanced Geotechnical Monitoring and Hazard Mitigation*, 1st ed.; Prasetyo, S.D., Muladi, M., Eds.; Acadlore Publishing Services Limited: Hong Kong, China, 2024; Volume 3, pp. 106–122.
12. Muladi; Wirawan, I.M.; Lestari, D.; El Raka, S.C.; Leksono, A.B.; Qodri, F.A.; Prasetyo, S.D. Chirpstack-Based LoRaWAN Platform for Land-Sliding Monitoring System. In *Instrumentation Mesure Métrologie*, 1st ed.; IIETA, Ed.; IIETA: Online, 2025; Volume 24, pp. 73–79.
13. Wang, C.; Guo, W.; Yang, K.; Wang, X.; Meng, Q. Real-Time Monitoring System of Landslide Based on LoRa Architecture. In *Frontiers in Earth Science*, 1st ed.; Oommen, T., Ed.; Frontiers Media S.A.: Lausanne, Switzerland, 2022; Volume 10, p. 899509.
14. Ragnoli, M.; Esposito, P.; Stornelli, V.; Barile, G.; De Santis, E.; Sciarra, N. A LoRa-Based Wireless Sensor Network Monitoring System for Urban Areas Subjected to Landslide. In Proceedings of the 2023 8th International Conference on Cloud Computing and Internet of Things, Okinawa, Japan, 22–24 September 2023; ACM: New York, NY, USA, 2023; pp. 91–97.
15. Bagwari, S.; Roy, A.; Gehlot, A.; Singh, R.; Priyadarshi, N.; Khan, B. LoRa Based Metrics Evaluation for Real-Time Landslide Monitoring on IoT Platform. *IEEE Access* **2022**, *10*, 46392–46407. [CrossRef]
16. Gamperl, M.; Singer, J.; Thuro, K. Internet-of-Things Geosensor Network for Cost-Effective Landslide Early Warning Systems. *Sensors* **2021**, *21*, 2609. [CrossRef] [PubMed]
17. Ragnoli, M.; Esposito, P.; Barile, G.; Ferri, G.; Stornelli, V. An Autonomous Multi-Technological LoRa Sensor Network for Landslide Monitoring. *Proceedings* **2024**, *97*, 11. [CrossRef]
18. Ioannides, M.G.; Stamelos, A.P.; Papazis, S.A.; Stamataki, E.E.; Stamatakis, M.E. Internet of Things-Based Control of Induction Machines: Specifics of Electric Drives and Wind Energy Conversion Systems. *Energies* **2024**, *17*, 645. [CrossRef]
19. LILYGO. *T-Beam—ESP32 LoRa/GPS Development Board*; Product Page; Shenzhen Xinyuan Electronic Technology Co., Ltd.: Shenzhen, China, 2025. Available online: https://lilygo.cc/products/t-beam?srsltid=AfmBOoqI2NdWZ6ygo87pIPBxoDN7r5e61jrLHtovKJPujVNijX8ESZA8 (accessed on 28 October 2025).
20. Semtech. *SX1276/77/78/79—137 MHz to 1020 MHz Low Power Long Range Transceiver*; Datasheet, Rev. 5; Semtech Corporation: Camarillo, CA, USA, 2016. Available online: https://www.mouser.com/datasheet/2/761/sx1276-1278113.pdf?srsltid=AfmBOoo_BWQqnOJi9DW8V_OUMfktcZUvheplPc1lnJ0NOIHJpl5aWOcN (accessed on 28 October 2025).
21. u-blox. *NEO-6—U-blox 6 GPS Modules*; Data Sheet GPS.G6-HW-09005-E; u-blox AG: Thalwil, Switzerland, 2011. Available online: https://content.u-blox.com/sites/default/files/products/documents/NEO-6_DataSheet_%28GPS.G6-HW-09005%29.pdf (accessed on 28 October 2025).
22. Analog Devices. *ADXL335—Small, Low Power, 3-Axis ±3 g Accelerometer*; Data Sheet Rev. B; Analog Devices, Inc.: Norwood, MA, USA, 2010. Available online: https://www.analog.com/media/en/technical-documentation/data-sheets/adxl335.pdf (accessed on 28 October 2025).
23. Panasonic Energy Co., Ltd. *NCR18650B—Lithium-ion Rechargeable Battery Cell*; Datasheet; Panasonic Energy Co., Ltd.: Moriguchi, Japan. Available online: https://www.tme.eu/Document/3e0170a1e089819f286f7066e69035b4/NCR18650B.pdf (accessed on 28 October 2025).

24. SparkFun Electronics. *Arduino Pro Mini 328 (5 V/16 MHz)*; Product Page; SparkFun Electronics: Niwot, CO, USA, 2025. Available online: https://www.sparkfun.com/arduino-pro-mini-328-5v-16mhz.html (accessed on 28 October 2025).
25. Hope Microelectronics (HOPERF). *RFM95W—LoRa Module*; Product Page/Datasheet; Shenzhen Hope Microelectronics Co., Ltd.: Shenzhen, China, 2019–2024. Available online: https://www.hoperf.com/modules/lora/RFM95W.html (accessed on 28 October 2025).
26. Intel Corporation. *Intel in California—Headquarters Information*; Intel Corporation: Santa Clara, CA, USA, 2025. Available online: https://www.intel.com/content/www/us/en/corporate-responsibility/intel-in-california.html (accessed on 28 October 2025).
27. Espressif Systems. *ESP32 Series—Wi-Fi & Bluetooth SoC*; Datasheet v3.9; Espressif Systems (Shanghai) Co., Ltd.: Shanghai, China, 2024. Available online: https://www.espressif.com/sites/default/files/documentation/esp32_datasheet_en.pdf (accessed on 28 October 2025).
28. Cadence Design Systems, Inc. *Xtensa LX6 Processor Core Architecture; Technical Overview*; Cadence Design Systems, Inc.: San Jose, CA, USA, 2017. Available online: https://arxiv.org/pdf/2106.10652 (accessed on 28 October 2025).
29. Microchip Technology Inc. *ATmega328P—8-bit AVR Microcontroller with 32KB Flash, 1KB EEPROM, and 2KB SRAM*; Datasheet Rev. 7810D–AVR–01/15; Microchip Technology Inc.: Chandler, AZ, USA, 2015. Available online: https://ww1.microchip.com/downloads/en/DeviceDoc/ATmega328P-Data-Sheet-7810D.pdf (accessed on 28 October 2025).
30. Pedley, M. *Tilt Sensing Using a Three-Axis Accelerometer*; Freescale Application Note AN3461, Rev. 6; Freescale Semiconductor, Inc.: Austin, TX, USA, 2007. Available online: https://www.nxp.com/docs/en/application-note/AN3461.pdf (accessed on 28 October 2025).
31. Luczak, S.; Oleksiuk, W. Increasing Accuracy of Tilt Measurements. *Eng. Mech.* **2007**, *14*, 143–154. Available online: https://www.engineeringmechanics.cz/pdf/14_3_143.pdf (accessed on 28 October 2025).
32. Thalmann, T.; Zechner, M.; Neuner, H. Accelerometer Triad Calibration for Pole Tilt Compensation Using Variance Based Sensitivity Analysis. *Sensors* **2020**, *20*, 1481. [CrossRef] [PubMed]
33. Semtech Corporation. *LoRa® and LoRaWAN® Technology Overview*; Semtech Corporation: Camarillo, CA, USA, 2025. Available online: https://www.semtech.com (accessed on 28 October 2025).
34. Semtech Corporation. *AN1200.22—LoRa™ Modulation Basics*; Application Note, Rev. 2; Semtech Corporation: Camarillo, CA, USA, 2015. Available online: https://www.semtech.com/products/wireless-rf/lora-connect/sx1278 (accessed on 28 October 2025).
35. Rabaça, A.F.B. Aplicação de Tecnologia LoRaWAN à Monitorização de Redes de Distribuição de Energia. 2018. Available online: https://fenix.tecnico.ulisboa.pt/cursos/meec/dissertacao/1972678479054034 (accessed on 20 May 2025).
36. The Things Network. Spreading Factors | The Things Network. Available online: https://www.thethingsnetwork.org/docs/lorawan/spreading-factors/ (accessed on 12 May 2025).
37. Etiabi, Y.; Jouhari, M.; Amhoud, E.M. Spreading Factor and RSSI for Localization in LoRa Networks: A Deep Reinforcement Learning Approach. *arXiv* **2022**, arXiv:2205.11428. [CrossRef]
38. XTAR. *18650 2600 mAh Li-Ion Rechargeable Battery*; XTAR: Shenzhen, China, 2025. Available online: https://www.xtar.cc/product/xtar-18650-2600mah-battery-69.html (accessed on 28 October 2025).
39. Inconshreveable, Inc. *Ngrok—Secure Introspectable Tunnels to Localhost*; Inconshreveable, Inc.: San Francisco, CA, USA, 2025. Available online: https://ngrok.com (accessed on 28 October 2025).